97 p.

I. DESIGN AND APPLICATION OF PIEZOCERAMIC TRANSDUCERS TO TRANSIENT PRESSURE MEASUREMENTS

II. SOME MEASUREMENTS OF CURVATURE AND THICKNESS OF REFLECTING NORMAL SHOCKS AT LOW INITIAL PRESSURES

Thesis by

Captain Douglas S. Johnson

United States Air Force

To become a part of Progress Report -
November 1, 1961 to May 1, 1962 -
NASA Grant NsG-40-60.

In Partial Fulfillment of the Requirements

For the Degree of

Aeronautical Engineer

California Institute of Technology

Pasadena, California

1962

ACKNOWLEDGEMENT

The work to be described herein would neither have been commenced nor completed without the continuous interest and guidance of Professor Hans W. Liepmann. Many helpful suggestions offered by Professors Albert T. Ellis and Julian D. Cole are gratefully acknowledged as well.

The patient and painstaking training on the operation of the 17-inch shock tube, conducted by Professor Bradford Sturtevant, was essential for the completion of this experimental program, as were the technical contributions of Mr. Lewis Balthasar and Mr. Thomas Johnson.

Miss Helen Burrus is responsible for the transformation of the manuscript from crude notes to its finished form, and the figures were created by Mrs. Nell Kindig and Mr. Ivar Tombach.

To all of the above especially, and to numerous interested friends who offered helpful advice and assistance during the course of this work, a deep debt of gratitude is acknowledged with sincere pleasure.

ABSTRACT

18139

A small pressure transducer, using the piezoelectric properties of a manufactured ceramic, was designed, constructed and installed in the end plate of the GALCIT 17-inch shock tube to obtain high-speed measurements of the pressure field behind a reflecting shock.

The design problem for piezoceramic pressure transducers and some possible solutions are discussed in detail. Results of transducer calibration and recommendations for improvement of the instrument are presented.

An initial program to determine the curvature of a shock at low initial pressures was run concurrently with calibration of five of the above pressure transducers. The results of this program are described in as much detail as the data obtained to date will permit.

At an initial pressure of 30 microns in the GALCIT 17-inch tube, the shock obtained at a Mach number of about 7.5 in argon is observed to have a total curvature of approximately 10 millimeters, or approximately two per cent of the tube diameter. The shock thickness observed under these conditions is approximately 5 millimeters. These results indicate that it may be entirely possible to obtain good optical measurements inside the shock, but that it may be necessary to resort to special techniques to avoid optical distortion caused by curvature.

TABLE OF CONTENTS

Section			Page
	Introduction		1
I.	Design and Application of Piezoceramic Transducers to Transient Pressure Measurements		4
	Part 1.	Initial Design Considerations	4
	2.	Piezoelectric/ferroelectric/piezoceramic Transducers	7
	3.	Transducer Construction	16
	4.	Transducer Calibration	24
	5.	Transducer Conclusions and Recommendations	30
II.	Some Measurements of Curvature and Thickness of Reflecting Normal Shocks at Low Initial Pressures		32
	Part 1.	Introduction	32
	2.	Experimental Equipment and Procedure	34
	3.	Data Reduction	37
	4.	Preliminary Results	40
	References		46
	Appendix A.	Transient Performance of a Piezoelectric Transducer	48
	Appendix B.	17-inch Shock Tube Configuration	59
	Appendix C.	Transducer Continuity Test Circuit	65
	Tables		72
	Figures		74

LIST OF TABLES AND FIGURES

Table		Page
1	Selected Piezoceramic Constants for Thin Disc Receivers	72
2	Selected Properties of Metals	73

Figure

1	Calculated Shock Rise Time, Pressure Step	74
2	Transducer Assembly and Sensitive Element	75
3	Bonding/Polarization Clamp	76
4	Shock Tube - Schematic	77
5	Instrumentation for Shock Curvature Measurements	78
6	End Plate and Damper Installation	79
7	Typical Calibration Traces	80
8	Transducer Calibration Curves	82
9	Typical Curvature Traces	83
10	Measurement Techniques	84
11	Typical Shock Shapes	85
12	Total Shock Curvature	86
13	Shock Thickness in Argon	87
14	Calibrated Test Gas Injection - Schematic	88
15	Driver Gas Mixture Technique	89

LIST OF SYMBOLS

To avoid confusion, those special symbols used only in the Appendices are not listed here but are defined as they appear, starting on page 48. The symbols listed below appear in the body of the text.

Subscripts for Shock Tube Notation

0	Ambient conditions: p_0 = 760 mm Hg; T_0 = 298°K
1	Test section initial condition
2	Condition immediately behind incident (primary) shock
4	Condition in driver at moment of diaphragm rupture
5	Condition behind reflected shock
s	Condition in, or pertaining to, shock wave
w	Condition near shock tube walls behind incident shock

Symbol	Definition
a	Speed of sound in a gas, meters/second
C	Capacitance, farads
D	Shock tube diameter, meters
g_{33}	Piezoelectric constant (See Appendix A and Table 1)
h_{ij}	Piezoelectric constant (See Appendix A and Table 1)
M_s	Shock Mach number
N_3	Frequency constant (see Table 1), meters/second
p	Gas pressure, usually microns of mercury column

LIST OF SYMBOLS (CONTD.)

Δp	Pressure jump: used herein as $\Delta p = p_5 - p_1$, mm Hg
R	Resistance, ohms (so noted when used)
R	Shock tube radius, meters
Re_w	Reynolds number at tube wall (see page 41)
r	Radial coordinate in plane of end plate, positive outward
r	Acoustic reflection coefficient (so noted when used)
S	Area, square meters
T	Gas temperature (note $T_1 = T_4 = T_0$ for all calculations), ^oK
U_s	Shock velocity, meters/second
v	Wave speed in solid (note $v = 2N_3$ for a thin plate) meters/second
x	Shock tube axial coordinate, positive <u>upstream</u> from end plate
x^i	Shock axial displacement at a given instrument location (see page 37), most conveniently in millimeters
x_w	Total shock axial bulge (see sketch, page 43), millimeters
X	Transducer ceramic thickness, millimeters
Z	Acoustic impedance (see page 14 or Appendix A) $\frac{\text{kilograms}}{\text{second}}$
γ	Specific heat ratio of a gas
δ_s	Shock thickness (see page 37), millimeters
ϵ	Relative dielectric constant of a material (footnote, page 11)
ρ	Density (of gas or solid), kilograms/meter^3
μ	Viscosity of a gas, kilograms/meter/second
λ_o	Viscosity mean free path, meters
τ	Time interval: (see page 37 and Figure 10), seconds

LIST OF SYMBOLS (CONTD.)

Abbreviations		Definition
cm	Centimeter:	10^{-2} meter
kg	Kilogram	
kc	Kilocycle:	10^{3} cycles/second
mc	Megacycle:	10^{6} cycles/second
mm	Millimeter:	10^{-3} meter
msec	Millisecond:	10^{-3} second
μ	Micron:	10^{-6} meter
μsec	Microsecond:	10^{-6} second

INTRODUCTION

The transition of flight vehicles from atmospheric operating conditions to near-complete vacuum environments, along with enormous increases in operating velocities, has made the detailed study of rarefied gasdynamics a matter of almost urgent practical interest. In particular, while significant results have been obtained demonstrating and explaining many aspects of shock wave behavior, the "thick" shocks typically formed in very low density atmospheres are relatively unexplored.

At least two reasons may be offered for the lack of experimental and theoretical work in this region. The first is a matter of scale; to obtain a suitably thick normal shock in which measurements may be taken, the size of the facility must be proportionately increased to maintain geometric similarity in the flows. The GALCIT[1] 17-inch shock tube (Ref. 1) was completed in 1961 to meet this requirement.

The second difficulty arises in instrumentation. A one-half inch thick shock, moving at about 10,000 feet per second, permits only about four microseconds for a fixed set of instruments to make their measurements. The demands generated for space and time resolution are evident, if meaningful data are to be obtained on the shock fine structure.

The first section of this paper reports results of a program to develop a pressure transducer with response time and sensitivity adequate to make such measurements. A piezoelectric system was

---

[1] Graduate Aeronautical Laboratories, California Institute of Technology.

considered the most promising from the considerations of simplicity, reliability, and performance. Five operating instruments, identical in all important respects, were finally constructed. The instruments were more or less specialized to operate flush with the end plate of the shock tube, since while a fully developed theory on the precise mechanism of shock reflection is not yet available, the boundaries are well defined and the experimental problem with existing instruments appears to be much simpler.

Information on the curvature of shocks in low-density media, besides being of great significance in itself in the formulation of theory concerning shock/boundary interactions, is needed to estimate the effectiveness of optical types of instrumentation for later experimental programs. Such data are fairly easily obtainable on the end plate, and in fact are very nearly independent of the exactness of response of transducers to pressure since only relative arrival times across the diameter need be measured.

The pressure transducer calibration series of shots was therefore broadened to gather a set of data on the curvature of a reflecting shock at initial pressures from 30 up to about 500 microns of mercury. Additionally, some rather interesting data on the thickness of a reflecting shock were obtained from the same shots. These results are reported in the second section of this paper and compared with data obtained by other investigators (Ref. 2, 3, and 4).

The usual difficulties associated with an equipment-development program arose. These, as well as some techniques and equipment

developed as a matter of convenience or enhanced accuracy of operation, are reported in some detail in the hope that such information may be useful to others involved in similar research with large-caliber shock tubes or piezoceramic transducers.

I. DESIGN AND APPLICATION OF PIEZOCERAMIC TRANSDUCERS TO TRANSIENT PRESSURE MEASUREMENTS

1. Initial Design Considerations

The problem of providing appropriate instrumentation to measure variations of pressure, both static and dynamic, in a fluid has been attacked almost exhaustively by investigators in every branch of the physical sciences. There is now sufficient theoretical background and experimental evidence on methods of measuring pressure to provide the prospective instrument designer with a broad spectrum of possibilities to meet his particular needs. The instrument he finally develops, if he selects his principles of operation carefully, may be limited only by his imagination.

A vast literature is available. A recent study by the Giannini Controls Corporation (Ref. 5) presents a good engineering survey of the entire field of pressure instrumentation, including a current bibliography of over 250 titles. Specializing to electrical input transducers for more or less continuous measurements of pressure, Lion (Ref. 6) surveys the field in detail, presenting brief explanations of the theory of operation and references to literature describing specific pieces of hardware. Specializing further to piezoelectric instruments, texts by Mason (Refs. 7, 8, and 9), von Hippel (Refs. 10, 11, and 12) and Hueter (Ref. 13) as well as numerous papers (Refs. 14, 15, and 16) explain the theoretical aspects of piezoelectricity and some of its applications to any desired level of complexity.

In spite of this imposing collection of documents on the subject, some discussion of the properties of piezoelectric transducers and other types of pressure instrumentation must be included here to explain the decisions leading to the transducer finally designed. The reader is referred to Appendix A for a detailed theoretical discussion following the methods proposed by Redwood (Ref. 14) of the transient performance of piezoelectric transducers.

The task at hand involved the design and construction of a transducer to obtain measurements of pressure as a function of time within and immediately behind a moving normal shock wave. The installation for which the instrument was to be designed was the GALCIT 17-inch shock tube end plate. Mach numbers up to 10 could be expected; the instrument should respond to pressure steps of the order of a few millimeters Hg. A response time of less than one microsecond was desirable.

Consideration of the transducer systems for which reasonably well developed literature was available led to the conclusion that, of the requirements mentioned above, the most severe limitation was imposed by the response time. An electronic readout system is obviously called for; hence the transducer has to be of the type which responds to pressure (or equivalently to force, strain, or displacement) by variation of a circuit parameter. Perhaps the fastest response times can be obtained with ion-current systems (Ref. 6), and they can be made extremely sensitive to very small pressure changes. However, most of the ionization gages developed actually measure density rather than pressure; thus an equation of state must be assumed, and

temperature known, to convert the reading to pressure. At Mach numbers where dissociation occurs, an equation of state is somewhat difficult to guarantee. Additionally, in an ionized gas attempts to measure pressure with a system dependent on a current flowing between electrodes may rapidly become meaningless.

Capacitance transducers can be constructed with response time adequate to meet the requirements. If properly shielded, ionization can be neglected. Sensitivity is adequate, and mechanical vibration in resonant modes, while present, is not much of a problem. This approach was rejected primarily because of the potential complexity of associated circuits, though Posel (Ref. 17) presents persuasive arguments in favor of the system and reports a capacitance transducer satisfactorily installed in a shock tube.

The field was thus narrowed to consideration of a piezoelectric effect to obtain the desired pressure measurements. In addition to reports on operating instruments by Mason and others mentioned above (though most of these are working at some resonant frequency), recent work by Willmarth (Ref. 18), Farrand (Ref. 19), and several Soviet authors (Refs. 20 and 21) gave every indication that the piezoelectric system was readily adaptable to shock tube work and, further, that the desired performance was attainable within the present state of the art.

2. Piezoelectric/ferroelectric/piezoceramic Transducers

A piezoelectric material is one that shows a displacement of electrical charge upon application of an external strain (Ref. 22). The process is reversible; application of an electrical field to such material will cause an elastic strain, and application of a field of the opposite polarity will change the sign of the strain components.

Consideration of crystal structure leads to the conclusion that all classes of crystals which do not have centers of symmetry should be piezoelectric. (Conversely, symmetric crystal structures cannot be piezoelectric.) About ten per cent of all crystals fall into the former category; those of commercial interest include Rochelle salts, quartz, tourmaline, ammonium dihydrogen phosphate (ADP), and potassium dihydrogen phosphate (DKT). It is interesting to note that most sugars are piezoelectric.

Within the general class of piezoelectric crystals are those containing dipoles within the unit cells. These types show a displacement of charge when heated, and are usually termed pyroelectric. Crystals which are both piezo- and pyroelectric can be polarized; that is, application of an electric field while the crystal is heated will cause a number of the dipoles to align themselves with the field. A crystal exhibiting this property strongly, and retaining a preferred polarization axis after cooling, is called ferroelectric. The temperature at which polarization is possible, or at which the dipoles of a polarized crystal revert to their lowest-energy orientation, is called the Curie point.

A polycrystalline aggregate of suitably ferroelectric materials (typically those having the formula ABO_3, where A and B are metals) can be prepared and fired by standard china-making techniques in any desired shape and a variety of compositions. When polarized, these materials possess piezoelectric properties of the individual components in an average sense. (Individual crystals of the aggregate are of course naturally piezoelectric before polarization, but their random orientation tends to cancel the effect on the macroscopic scale.) These materials are the piezoelectric (or ferroelectric) ceramics or, in the interest of brevity, piezoceramics. Typical compounds now commercially available include barium titanate (with or without certain calcium, phosphorous, lead, zirconium and titanium additives) and the PZT series[1].

The piezoceramics generally show stronger piezoelectric effects than the natural crystals. Additionally, their composition can be varied to minimize second-order effects (typically to make the polarization vs. temperature curve flat over a larger range of temperature) or enhance desired characteristics such as certain elastic constants or the dielectric constant. Since they are molded and fired in any shape desired, the problem of cutting parallel to certain crystallographic axes is eliminated. Finally, the possibility of radial, helical and other polarizations is unique to the ceramics.

---

[1] "PZT" is a registered trademark of the Clevite Corporation, Cleveland, Ohio. It is a generic name for a family of lead zirconate/lead titanate ceramics.

Appendix A includes a brief discussion of the various piezoelectric constants and the equations with which the piezoelectric effect is usually defined. Table 1 lists some of the more useful of the piezoelectric constants. Of these, the piezoelectric "stiffness constant" h_{ij} is most useful to define the sensitivity of a ceramic in a simple application, since it relates the elastic and electrical properties of the material in a dimensionally convenient fashion (in rationalized MKSC units)[1].

It should be noted that the dipole alignment resulting from the polarization process[2] is only statistically greater along the axis of polarization. The other piezoelectric constants are not identically zero, though they are slightly suppressed. If electrodes are only applied to two parallel surfaces of the polarized geometry, six of the nine h_{ij} can be ignored in considering the response of the transducer.

The response time of a transducer, as indicated in Appendix A, depends on the appropriate elastic wave speed in the material and the distance between electrodes. In the case of the thin circular disc transducer polarized normal to the flat faces, this time can be minimized by making the ceramic element as thin as possible.

However, as Willmarth (Ref. 16) points out, the sensitivity of the element is directly proportional to its thickness. The operating sensitivity of a transducer may thus be limited if it is designed solely

---

[1] There is a considerable lack of uniformity in the notation of older texts. The IRE Standard (Ref. 16) is now generally used by the industry, and is strongly recommended to resolve the confusion arising in a literature search on this subject.

[2] An excellent discussion of the polarization process is given by Hueter and Bolt (Ref. 13, page 249). Willmarth, however, disagrees on the polarization potential and time required.

from rise time considerations. The expected operating range of the transducer, in terms of amplitude and wave form of the input signal, should be calculated to arrive at the necessary design compromise. (For an example, see Figure 1).

In designing the transducer assembly some thought must be given to the effect of geometry on the response time. When a stationary instrument is used to sense pressures in a moving shock, the orientation of the instrument with respect to the shock is of profound importance. An instrument used in the side wall of a shock tube will be restricted in at least one dimension beside the thickness since the time response will be determined by the time required for the shock to sweep across the sensitive face. Obviously the most favorable situation from this point of view is for the smallest dimension and the axis of polarization of the transducer to coincide with the axis of propagation of the shock wave. However, one must then accept measurements of pressure conditions behind a reflecting shock or, in the case of a small diameter instrument inserted some distance into the tube, behind a standing "bow" shock after it is formed. Gasdynamic considerations (Ref. 23) show that the transducer, merely by its presence in the flow, may alter the pressure conditions measured.

The <u>electrical circuit parameters</u> of the transducer will have some effect on its performance as a function of time. In particular, the static capacitance of the crystal and the resistance and capacitance of the loading circuit are intimately connected with transducer response. The electrical characteristics of the materials used

to bond the sensitive element to its support system may have a direct influence in transducer performance as an assembly. Stray resistances or capacitances in the assembly can alter the signal.

The resistivity of most piezoelectric materials is typically very high (order of 10^{12} ohm cm). Capacitance varies widely with the materials used; quartz has an extremely low dielectric constant, about 4.5 while the piezoceramics have constants ranging from 1000 up to about 3000 referred to the dielectric constant of free space[1]. Since the voltage generated by a given charge is inversely proportional to the capacitance between the charged plates, the dielectric constant of the material will influence the sensitivity of the output. It may therefore be desirable from this point of view to choose a material with the lowest possible dielectric constant.

On the other hand, the circuit decay time constant is determined by the product (RC) of the ceramic static capacitance, considering also the capacitance of connecting circuits, and the input resistance of the loading circuit. For fast transient signals, it is desirable to make this number as large as possible, typically greater than 10^{-4} seconds for work in the microsecond region. This consideration argues for either a relatively high dielectric constant or extremely high input resistance (order of 10^{8} ohms), especially if low frequency response is to be preserved. Again a design compromise is indicated.

---

[1] $\epsilon_o = \frac{1}{4\pi \times 9 \times 10^9}$ $\frac{\text{farads}}{\text{meter}}$, and for a particular capacitor $C = \epsilon\epsilon_o \frac{S}{X}$ farads, where ϵ is the dielectric constant, S is an appropriate plate area, and X is the distance between plates.

Finally, a number of important mechanical considerations influence the transducer design. Some of these, such as the elastic and mass constants of the ceramic element, affect sensitivity and response time directly. When the supporting structure is considered, a number of additional effects may influence the output wave form.

The work by Kolsky (Ref. 24) covers elastic waves in solids in some detail. More recently Miklowitz (Refs. 25 and 26) has expanded the theoretical foundations of the subject to the point where the engineering problem is quite well defined. The effects of primary importance are mechanical impedances of ceramic element and support system, primary modes of natural oscillation, and elastic wave speeds. Secondary effects include discontinuities (cracks, bubbles, scratches); higher vibration modes, and dispersion.

The input pressure wave form can be approximated over a small interval by components of a series of periodic functions. (Ref. 13, page 380, for example; or see any good text covering Fourier analysis). Qualitatively, an infinitely thin shock will contain an infinite spectrum of frequency components, and the high-frequency terms will be of large amplitude. As the shock thickens, the high-frequency terms are of less importance. In fact, a $\frac{1}{2}$ cm thick shock impinging on a plane normal to its direction of propagation at 2500 meters/second appears to contain no significant terms higher than 400 kilocycles. A shock one tenth as thick at the same speed may contain components up to a few megacycles.

Working with the thicker shock, ringing frequencies of order 1 megacycle can safely be ignored; they will not be excited. However, an instrument designed from this point of view may suffer considerably in performance when thinner shocks are obtained. (It is interesting to note that this effect works both ways; an instrument based on a number of tuned reeds to take advantage of a spectrum of ringing frequencies could be used to reconstruct a Fourier series representing the incident shock. Some fairly formidable digital computer work might result.)

Additionally, a thick shock will suffer less from dispersion in a metal rod, say, and will be more faithfully reproduced at the far end than one containing a number of high frequencies. The ratio of rod length to diameter and a well-defined sonic velocity are important parameters here; see Kolsky.

Depending on the input wave form, the output signal may contain components representing fundamental and harmonic vibrations of the ceramic sensitive element itself, its immediate support system, and surrounding mechanical elements. In the particular case of a cylindrical, thin ceramic wafer bonded to a relatively long metal rod which in turn is attached to the shock tube by an appropriate mounting, the following effects are observed with a thin shock as defined above.

The highest frequency component (order 5 megacycles) is due to reflection of the stress pulse at the ceramic/metal interface, and its frequency is given by the sonic velocity and thickness of the ceramic disc. The amplitude of this component is determined by the value of

the reflection coefficient r, which for any boundary is defined as (see Appendix A)

$$r = \frac{Z_2 - Z_1}{Z_2 + Z_1}$$

for a wave traveling from medium 1 into medium 2. The quantity Z is the acoustic impedance of the substance, and its value is given by the sonic velocity v, density ρ, and area S as

$$Z = \rho v S \qquad \text{kg/sec} \qquad \text{(MKS units)}$$

An impedance match is obtained when r is zero. A perfect mismatch is obtained when $r = \pm 1$. Note that this is the familiar condition at a "free" boundary of a solid; $Z_2 \ll Z_1$ and a compression pulse is reflected as a tension wave.

Fundamental ringing of the ceramic element can thus be eliminated by backing it with a material which will provide a good impedance match.

The next significant component (order 500 kc) appears to be a radial ringing in the crystal and supporting rod. Using the shear velocity, the wave length of this oscillation is just the diameter of the rod. This is a second-order effect due to the Poisson's ratio of the material. Damping is somewhat uncertain and the resulting modulation of output signal can be a nuisance. This effect can be minimized, if suitably thick shocks are to be measured, by selecting a diameter small enough so that the mode is not excited by the input pressure function.

A component of order 50 kc is generated by reflection of the stress pulse from the far end of the supporting rod. This frequency

can be adjusted rather easily by lengthening the rod and some damping may be possible by varying the rod support system. It should be noted here that surface flaws on the rod will reflect pulses; these in general are small and fairly well damped.

Finally, the whole transducer housing may vibrate at several different frequencies between 50 cycles and about 5 kilocycles. These effects are unimportant in the wave form observed at sweep speeds of 1 μsec/cm, since the interesting higher frequencies simply modulate these signals. If, however, these oscillations are large enough the "galloping zero" problem may arise making high-speed oscillography somewhat more complicated. This effect is discussed in part 4 of this section.

The transducer assembly must be compatible with the vacuum system of the shock tube. From the mechanical point of view, this requires provision of a vacuum seal somewhere in the transducer housing. While this is not exceptionally difficult to accomplish, the designer's choice of techniques may exert a profound influence on the performance of the transducer as a vibrating system.

To summarize this discussion, piezoceramic transducers offer a definite advantage in fairly high sensitivity, good response time, and great flexibility of application. There are some potential disadvantages in the intimate coupling between mechanical and electrical characteristics of such transducers[1] however, and the designer is well advised to proceed with caution.

---

[1] Though not discussed here, there are second-order thermal, electrostatic and electromagnetic characteristics which may sometimes be significant. See Reference 22, page 450.

3. Transducer Construction

Some satisfaction could perhaps be derived from a statement that all the material in the previous section was considered before design was started on the specific instrument next to be described. Such, unfortunately, is not the case. The instrument and the material of the previous section evolved more or less concurrently through a lengthy trial-and-error process, and a number of attempts were discarded before the final instruments were ready.

The final transducer design is shown in Figure 2. The sensitive element is a PZT-5B[1] wafer 0.125 mm thick, 5 mm in diameter, acoustically bonded in a brass rod of the same diameter and 85 mm long. The rod, in turn, is radially supported along its whole length by a silicone rubber[2] plug of 5 mm i.d., 25 mm o.d. molded to fit tightly inside a stainless steel container. The assembly then replaces the pyrex plug of the thin film heat gage shown in Figure 6, Reference 1 in the standard instrumentation plug of the 17-inch shock tube.

Tables 1 and 2 list selected properties of piezoceramic materials and some metals respectively. It appears that the derived quantity $g_{33}N_3$, with units $(\frac{\text{volts/second}}{\text{newton/sq meter}})$, may be a useful measure of the pressure sensitivity and response time of a piezoceramic since it is dimensionally independent of ceramic thickness.

---

[1] A lead zirconate-titanate compound with some other additives to stabilize the polarization, manufactured by the Clevite Corporation, Cleveland, Ohio.

[2] Dow Corning Silastic RTV 501.

The systems tested most extensively were barium titanate discs on zinc rods and PZT-5B discs on brass rods. The PZT/brass combination was chosen as the final design for several reasons, including the trivial (but frequently decisive) one that the PZT was readily available, pre-polarized, in sheets 0.25 mm thick.

The optimum configuration for the ceramic element for work on the shock tube end plate is obviously a thin disc parallel to the plane of the shock. A thickness of about 0.2 mm was selected to give a response time of order 0.05 μsec. The technique of acoustically matching a single disc to a rod of the same diameter, suggested by Zaitsev (Ref. 20), appeared most promising to eliminate undesirable oscillations.

The discs were cut from a sheet of pre-polarized ceramic with silvered surfaces, using a brass cutting tool in a small drill press[1]. The rods were machined from rolled bar stock. No attempts were made to relieve machining stresses in the rods, and this does not appear to be necessary.

Discs and rods were lapped to optical flatness to obtain reliable acoustic contact. This is a tedious but critical part of the assembly process. The lapping removes the silver from one surface of the ceramic; this is of little consequence since the charge collects on the surface whether or not the electrode is there. The matching surface of the rod serves as the electrode, and the rod itself is the conductor with which the signal is removed from the crystal.

---

[1] See Willmarth (Ref. 18) for details of this technique.

Careful inspection with a suitable microscope (30X is adequate) and meticulous cleaning of the lapped surfaces before bonding is also essential. The most satisfactory cleaning technique involved gentle polishing with an impregnated cloth to remove the lapping compound, followed by careful rinsing and scrubbing with xylene, acetone, and ether (in order). It appears that scratches visible under a 60X microscope (but not to the naked eye) are of little consequence; they certainly cause small local variations in the thickness of the bonding layer but no measurable loss in its acoustic quality.

A number of bonding compounds, mostly expoxide-base cements, were tried. Of these, a pure dielectric[1] (non-conducting) offered the most strength, but it turned out that its capacitance in series with the ceramic wafer reduced the output of the transducer assembly by a factor of 5. Additionally, circuit analysis shows immediately that the voltage response of such a system is highly frequency-dependent. A silver-bearing conducting cement[2] was finally chosen as the most satisfactory considering strength and resistivity. The fact that it had to be cured at about 150°C was one of the factors leading to the final selection of a ceramic with high Curie temperature since the very thin ceramics turned out to be extremely difficult to re-polarize -- an undetectable internal flaw quickly reduces the breakdown voltage to a value lower than that required for polarization and the ceramic burns through.

---

[1] Eccobond 26.

[2] Eccobond 58C. (A two-part cement which cures at room temperature -- Eccobond 57C -- offers the same mechanical and electrical properties according to the manufacturer but showed extreme weakness in shear. This may have been due to the age of the sample or improper mixing technique on our part.)

The flat surfaces of the rod and ceramic were coated with a thin layer of the conducting cement, using dental tools and working under a microscope to detect dust and other particles. The elements were then pressed in a clamp (Figure 3) and cured at the temperature recommended by the cement manufacturer for a minimum of 24 hours. (The clamp may be insulated to permit simultaneous polarization - this technique worked very well with ceramics thicker than about 0.2 mm.) The original ceramic disc was slightly larger than the rod; after bonding, a uniform diameter was obtained and excessive cement removed by machining with abrasives.

A few miscellaneous notes on this bonding technique may be of interest. The cured cement layer is about 0.01 mm thick and very uniform. Excess cement is squeezed out nicely by the clamp (pressure is about 75 kg/sq cm) and a better bond is obtained if the cement is not thinned. The ceramic manufacturer warns of a permanent loss of some percentage of the pre-polarization if the ceramic is heated to within 100°C of the Curie temperature. This effect, if present, is too small to observe in the assemblies constructed here. When polarizing the ceramic, the face which will see the shock wave first is connected to the negative terminal of the power supply in order to obtain a positive voltage response to rising pressure when the completed transducer is in operation.

A silicone rubber plug was chosen to hold the sensitive element (which in further discussion will refer to the ceramic disc bonded on the rod) for several reasons. The basic functions to be performed are

fixing the sensitive element in space and providing a vacuum seal. A secondary consideration is the need for isolation from vibrations in the shock tube structure. In addition, there is a strong possibility that wave reflections will be set up at points of support of the rod - this indicated either a cantilevered rod or a continuous but loose support. Finally, the fact that the transducer was in a development program suggested that the support system be easily disassembled for either minor adjustments or complete replacement of the sensitive element.

The plugs were molded in special brass cans to obtain an outside diameter of 23 mm. The stainless steel cans in which they were later inserted had an inside diameter of 22.5 mm; this difference in diameters allowed for approximately 1 per cent shrinkage of the rubber after cure and provided an adequately tight fit to make a vacuum seal. All metal surfaces were finished smooth. The brass and steel cans were otherwise identical in dimensions. A rod was inserted in each mold, located along the axis with a small fixture, to provide the space for the sensitive element to be inserted. The last 15 mm of the rod was threaded, and a nut was thus molded into the rubber plug (see Figure 2). The silicone compound was mixed according to the manufacturer's instructions, poured into the mold, and immediately placed under vacuum for at least two hours to allow air bubbles and trapped volatiles to escape. It was then cured at about 65°C for a minimum of 24 hours, removed from the mold and cured another 12 hours, and finally pressed into a stainless steel can. A small amount of vacuum grease was used on the outside of the rubber;

originally the sensitive elements were greased also, but later it was found that this was placing a leakage resistance across the ceramic and adversely affecting the signal. The rubber plugs in the final design were carefully cleaned inside before the rods were inserted; vacuum leakage is prevented only by the slight compression of the rubber (the sensitive elements were about 1 per cent bigger than their corresponding holes).

Microscopic examination of cut-up samples of the silicone plugs showed that the vacuum molding technique was quite beneficial in producing a plug of uniform composition, virtually free of bubbles. A compound which cured much faster (about 4 hours) was tried, but it was found that the cure commenced so rapidly after mixing that the vacuum technique was unable to remove all the bubbles before the rubber was too well set to prevent their escape.

The leakage resistance mentioned above proved to be quite a large factor in the final signal output. All traces of oils and grease -- even fingerprints -- had to be removed from the rods and the inside surface of the rubber plug during final assembly. The most satisfactory solvent for this purpose turned out to be ether, probably because it leaves the least residue and evaporates very quickly.

The adequacy of the rubber plugs in the shock tube vacuum system and as vibration dampers will be discussed in part 4 of this section.

The "ground" contact for the transducer is made between the front face of the sensitive element and the stainless steel can with

silver paint. On several of the models tested, this paint was applied in a uniform thickness of about 0.025 mm with an airbrush. This provided satisfactory contact, but was quite susceptible to any movement of the rubber sleeve it covered, and contact might be lost after a few shots. In later models, addition of a narrow strip of Mylar tape as shown in Figure 2 solved the problem.

The transducer assembly, now including sensitive element, rubber plug and steel can, is mounted in the standard instrument plug for the shock tube. A tight O-ring fit around the outside diameter of the can makes the vacuum seal; the can is held firmly in place with a nylon clamp. The clamp, in turn, is bolted to the plug. The final models supported the nylon clamp on a stack of O-rings and washers to provide better shock mounting.

The transducer circuit was a matter of some concern, since almost all investigators have used cathode followers with their instruments. To check the need for such a circuit in the range of operation desired, one was built using the circuit designed by Willmarth (Ref. 18) and connected to several configurations of the transducer during its development. No noticeable difference was observed in the output signals, and the conclusion was reached that since the capacitance of the ceramic itself was so high (about 1.2×10^{-9} farad) the circuit time constants were such that an input resistance of 1 megohm was adequate. Additionally, frequencies below about 10 kc were of little or no interest in the application of the transducer.

Satisfactory circuit performance was obtained with ordinary Amphenol connectors and RG-62/U coaxial cable. The shield of the cable was grounded at the shock tube with one side of the ceramic element. Cable lengths of up to 12 feet produced no noticeable change in the signal.

4. Transducer Calibration

Most of the transducer calibration work was carried out in the 17-inch shock tube, with the instruments installed on the end plate (Figure 6). The current configuration and operation of the tube is covered in Appendix B. Figures 4 and 5 show the tube layout and instrumentation block diagrams.

There are both advantages and disadvantages to pressure transducer work on the end plate. Among the advantages in a calibration series are the conditions naturally occurring behind a reflecting shock. The pressure between end plate and reflected shock is higher for a given incident Mach number than anywhere else in the tube, instantaneously; this may avoid the necessity for preamplifiers during transducer development. More important, the shock reflects from a sufficiently small area all at once; thus only one dimension (e. g. the thickness of the ceramic disc) is important in determining the response time of the transducer. The pressure step on the end plate (hence on a flush-mounted instrument) can be calculated with some certainty up to incident shock Mach numbers of about 6 from ideal gas theory, and with suitable tables and charts (for example Ref. 27) up to higher Mach numbers.

Figure 1 presents the results of such a calculation, using air as the driven gas with a helium driver. Driver pressure is constant along each curve, while Mach number is permitted to vary. It was somewhat surprising to obtain a nearly straight line on a logarithmic plot suggesting a simple power law relation between Δp and p_1, since the

calculation was done numerically in several steps and this result is not at all obvious.

The first transducers calibrated were constructed as described in part 3 of this section, except that the rubber plugs were not made to fit tightly in the steel cans and the front faces of the ceramic elements were exposed directly to the shock, uncovered except for a very thin layer of sprayed silver paint. Problems with leakage around the plugs led first to heavy applications of vacuum grease and compression of the plugs with nylon caps. Later the technique of molding the rubber slightly oversize proved to be the best fix and both grease and caps were discarded.

A more serious problem with these instruments (most were barium titanate, 0.5 mm thick, with zinc backing rods) was that their response did not appear to be stable after initial shock impact. The instruments did respond to the shock, but then the traces observed on a longer time scale (10-20 μsec/cm) continued a relatively slow monotonic rise, with some sinusoidal modulation, to a much higher value. Re-examination of the theory presented in Appendix A led to the conclusion that the time constants of Equation 36 were such that the primary effect on the output signal was the exponentially rising term of Equation 40.

It appeared that the most effective way to modify the time constant was to change the reflection coefficient at the front face of the ceramic from 1 to a value as nearly zero as possible; that is, to provide an impedance match on the front, as well as the back, fact of the ceramic. Equation 43 of the one-dimensional theory should predict the performance of the transducer for this case.

This first part of the calibration program also provided information on the ringing frequencies of the assembly. Of the several modulations observed, the only strong one had a remarkably consistent frequency of 400 kc. A number of variations of the ceramic geometry (notched edges, triangles, smaller diameter discs, etc.) were devised to eliminate this signal - all without much success. Since the diameter of the backing rod was not varied, the conclusion is drawn that the effect comes from radial vibration of the rod itself. Reference to the detailed wave propagation theory of solid rods (Ref. 24, page 75) justifies this and explains the inability of the one-dimensional approach of Appendix A to predict the effect. Note also that the ceramic is responsive to shear waves as well as the primary longitudinal one.

The transducers were modified at this point in the program to make the front face impedance match suggested above. This was done by acoustically bonding a brass disc, 1.5 mm thick, to the front face of the crystal, using the techniques outlined in part 3 of this section. The finished product is illustrated in Figure 2. After the four lapping and two bonding operations, the whole assembly was carefully machined with abrasives and polished so that the ceramic was only discernible as a thin line of different color interrupting the otherwise uniform brass rod.

The brass discs on the front faces may be thicker than necessary. One of the reasons for the selection of this thickness was the hope that if the 400 kc vibration was a surface effect it would be better damped if the wave was forced to travel a short distance before striking the ceramic. Some dispersion of the wave may have been introduced, but the results of shots to check the response time of these instruments

indicates the effect is small. The impedance match did solve the problem of the monotonically rising signal, but did little to the oscillation.

Typical traces from the transducers finally developed are presented in Figures 7 and 9. Pressure and Mach number conditions are indicated with each trace. Comparison with the shock rise time lines sketched on Figure 1 shows that the instruments do follow the shock up to rise times of about 0.1 μsec, where a discontinuity in the slope of the rising trace is observed. This is taken as a good indication of the limiting response speed of the instrument. Faster rising shocks, especially those of large amplitude, show a definite bright spot at the same point on the trace. A very small signal with a frequency of about 5 mc occasionally appears on these traces as well.

It is interesting to note that the spots on the rising traces, which are quite typical of transducers with front plates or diaphragms, were not observed on those models where the front face of the ceramic was uncovered. It is quite possible that the effect is due to the limiting frequency which can be passed by the (viscoelastic) bonding layer on the front face, rather than a direct effect of the ceramic itself. The spot is thus a reflection in the bonding layer.

The point at the peak of the trace was selected as the correct voltage to use in calibration curves. Figure 8 shows the curves for five instruments.

Perhaps the most annoying oscillation noticed was the "galloping zero", caused by the response of the end plate itself to the stress pulse in the metal of the tube. The effect is somewhat noticeable in Figure 9,

where the base lines of the traces are displaced from their intended starting positions. In fact, several traces were lost entirely during the calibration runs.

Figure 7d shows the effect clearly. A simple calculation based on the assumption that a pulse in the metal traveled from the bursting diaphragm at about 5 mm/μsec while the shock moved in the gas at half that speed showed that the end plate should start vibrating about 4 msec before the shock arrives. It turned out that this is almost exactly the case. The fundamental frequency of the plate is about 500 cycles, and a 5000 cycle signal is superimposed.

The transducer cans were re-mounted on stacks of O-rings to provide a softer shock mounting. This eliminated the 5000 cycle component completely. However, since the sensitive elements have (relatively) large masses on both sides of the ceramic, they function very well as accelerometers and the 500 cycle oscillation is more or less undisturbed.

Of the possible solutions to this problem, the most effective would certainly be a complete isolation of the end plate from the pulse in the tube - perhaps by addition of a rubber section to the tube. Another possibility, economically somewhat more feasible, would be construction of a new, lighter, stiffer plate. The most satisfactory interim solution to the problem was the addition of a stiffening and damping arrangement to the existing instrumented assembly (Figure 6). This consists of two large wooden blocks, four inches square and as long as the plate diameter. These are clamped tightly against the end plate just above and below the line of transducers by another heavy

steel plate (in fact the original "blank" end plate for the tube). This in turn is bolted to the tube end flange with bolts extending through, but not touching, the instrumented plate. This arrangement has cut the amplitude of the 500 cycle component approximately in half.

The rubber plugs are apparently quite adequate to hold the transducer sensitive elements in place. They certainly contribute some damping to the shock-excited motion of the sensitive element, and do not introduce reflections in the rod. They provide some degree of vibration isolation, especially for frequencies above a few kilocycles. However, the large amplitude, low frequency vibrations of the thin end plate presently installed are not well damped, and the use of preamplifiers to extend the useful range of the transducers to lower pressures may be considerably limited by an inability to keep the traces on the screen. (Except for the 500 cycle component, the transducer signal-to-noise ratio is good enough to permit the addition of a factor of ten gain to the system.)

The rubber plugs are satisfactory vacuum seals without grease or other sealing compounds. The leak rate of the tube, measured daily over a 12-hour period with all instruments installed, is consistently less than 0.05 micron/hour. Only a small area of the rubber is exposed to the vacuum, and out-gassing has not been a problem.

5. Transducer Conclusions and Recommendations

No claim will be made that the above transducer design is either optimum or unique. The instruments described above are adequate for work on the shock tube end plate at initial pressures between about 10 and about 500 microns (in air; the upper limit is about 20 per cent higher in argon) at a nominal Mach number of 7 or 8. Typical sensitivity for these units is 0.3 millivolt/mm Hg pressure step. Limiting response time is about 0.1 microsecond.

Extraneous noise modulating the shock-excited output signal has been minimized, except for the 400 kc ringing of the backing rod, and for sufficiently thick shocks this is only weakly excited. The instruments are a little too sensitive to large amplitude, low frequency accelerations.

The limiting response time of 0.1 microsecond, as mentioned above, may be due in large part to the addition of a front plate to the ceramic face. The plate did solve the problem at hand, but there may be a better solution which permits the front face of the ceramic element to be exposed.

The silicone rubber plug is a useful feature of the instrument. In addition to its primary functions as vacuum seal and vibration isolator, it contributes substantially to the ruggedness of the assembled unit.

Several recommendations, based on operating experience with the instruments, may be of value in future design consideration.

a. The front face of the ceramic should be left uncovered if at all possible. Improved sensitivity (a factor of about 2) and better response time may result. If the front surface must be covered, an

extremely thin, smooth conducting surface plated or sputtered on may give better performance than the Mylar tape and silver paint.

b. A large reduction of rod diameter should drive its natural frequency up to the point where it is not excited by thick shocks. Some judicious scoring of the rod surface to generate mutually canceling reflections may be useful.

c. For investigation of shocks with a rise time of order two microseconds, the proper adjustment of ceramic thickness may provide more sensitivity with a reasonable response time of about 0.2 μsec. It should be noted that simultaneous increase of thickness and reduction of diameter will reduce the static capacitance of the ceramic, hence change time constants.

d. Better acceleration compensation of the instrument housing will permit the use of preamplifiers and extend the useful range of the instrument. Preamplifiers are presently not feasible because of the "galloping zero" problem. Construction of an end plate of nylon or a similar material may be useful.

e. The rubber plug can be improved somewhat. In particular, the sensitive elements should be completed, tested, then potted in individual plugs to obtain the most uniform radial loading of the backing rod.

II. SOME MEASUREMENTS OF CURVATURE AND THICKNESS OF REFLECTING NORMAL SHOCKS AT LOW INITIAL PRESSURES

1. Introduction

The limitations on shock tube performance at very low initial pressures appear to arise primarily from effects largely ignored in the usual one-dimensional theory. Viscosity and thermal conductivity contribute strongly to such effects, and an interaction between shock, boundary layer, and contact surface may seriously impede experimental progress in certain cases.

In particular, at low densities it can no longer be assumed that the shock is plane, and this effect arises mostly because the tube walls are present to constrain the flow. Large caliber shock tubes have been completed recently to maintain geometric similarity at the low densities (Refs. 1 and 4), but without a clear understanding of the precise mechanisms of shock/boundary layer interaction it may be dangerous to assume that a bigger tube automatically permits extension of the ideal shock tube theory.

Shock curvature is interesting to study for at least two reasons. First, it may be possible through detailed study of the shock shape to determine the mechanism of shock/boundary layer interaction more accurately, and perhaps gain further insight on the construction and motion of the contact surface as well. Second, those investigators intending to use optical instruments to look at the fine structure of a thick shock must regard data on curvature as a most critical element of their instrument design.

Hartunian (Ref. 2) has formulated a two-dimensional theory of shock shape which may be at least a starting point for theoretical explanation. Experimental data have been obtained by Duff (Ref. 3) and Lin (Ref. 4) confirming the existence of curvature but agreeing only qualitatively with Hartunian.

Lin worked with air in a 24-inch shock tube, obtaining data on total curvature as an "apparent shock thickness" with an optical instrument aimed across the tube. Duff used argon in a 1.5 inch tube, taking measurements in the same manner as those to be presented here. Qualitatively at least, one might expect curvature measurements in argon in a 17-inch tube to bear some similarity to both sets of data.

The measurement of shock curvature is most simply obtained with instruments mounted flush in an end plate. Some indications of the thickness of the reflecting shock appear as a fringe benefit in this investigation, and the questions of shock symmetry, instability or "tilt" are considered.

2. Experimental Equipment and Procedure

The experimental program to measure curvature and thickness of a reflecting shock was carried out concurrently with the transducer calibration series reported in Section I of this paper. Five pressure transducers (Fig. 2) were flush mounted in a stainless steel end plate (Fig. 6) at various stations along one diameter of the plate. Two of these stations were redundantly located, providing a check on the symmetry of the shock. Thin film heat gages (Ref. 1) were used along the side walls of the tube to obtain shock velocity measurements and to trigger the electronic recording systems.

Each shot generated data on the shock history, its curvature and thickness, its symmetry, and a pressure calibration for the instruments. For curvature measurements, the only information taken from the transducers was the arrival time of the shock. For thickness, the maximum slope was taken from the earliest part of the rising trace to obtain a time differential representing shock rise time.

Most of the runs were made at a Mach number of 7.35 ($\pm$ 0.20) in argon, with initial pressures ranging from 30 microns Hg up to one millimeter. Details of shock tube operation are presented in Appendix B. A purging procedure prior to each shot assured gas purity. Mach number was held constant as initial pressure was increased by decreasing the partial pressure of nitrogen in a helium/nitrogen driver gas mixture. Driver total pressure was held constant at 18 psig.

Outputs from the thin film heat gages mentioned above (taken in pairs) were differentiated, amplified, and presented to microsecond

counters[1] which then indicated directly the time required for the shock to traverse 500 mm at stations located about 1, 10, and 19 tube diameters upstream of the end plate. The last film gage, 200 mm upstream of the plate, was used to trigger the oscilloscope system.

Figure 5 is a block diagram of this system. Three oscilloscopes[2] and a fast pulse generator[3] are the major components. The trigger signal from the film gage was used to start a delay generator. This unit fired a trigger pulse after a preset time (typically 80 μsec) to start sweep generators in all three oscilloscopes and another delay circuit in the pulse unit. After a 9 μsec delay, the pulse generator produced a very fast rising 100 volt square pulse of about 10 μsec duration. This was presented directly to the CRT cathodes of all three oscilloscopes as a blanking signal (the manufacturer calls this technique "Z axis modulation"). This served as a common time marker for all traces.

All instruments were set up for single sweep operation, and the usual Polaroid camera techniques with 3000 speed film were used to obtain pictures of the traces. Sweep rates were checked periodically and assumed accurate within 1 per cent otherwise. A sweep of 1 μsec/cm was usually used. A maximum vertical deflection sensitivity of 5 millivolts/cm was available with the installed oscilloscope preamplifiers. A typical set of the traces obtained for each shot is presented in Figure 9.

---

1 Beckman/Berkley 7200 and 7300 series; various models.

2 Tektronix 535A (single beam); 551 and 555 (dual beam).

3 DuMont type 404.

There is little point in dwelling on the complexities of high speed oscillography; they are well known. The data desired in this experiment required completely synchronous operation of three oscilloscopes, and it turns out that there is a residual uncertainty of starting time of at least 0. 1 μsec with the sharpest obtainable trigger signal. The time mark was essential to compensate for this error, and the intensity modulation technique was quite successful.

It is interesting to note that the shock obtained at 30 microns in argon is curved enough to make a span of 9 microseconds from the beginning of the first trace to the peak of the last. At 1 μsec/cm, a total of only 10 microseconds sampling time is available. Outside of the fact that this required prediction of delay time settings in the trigger circuit[1] to an accuracy of one per cent (the manufacturer only guarantees three per cent), this means that a major program of electronic instrumentation will be required to use this sampling technique to the same accuracy with lower pressures. Some runs at 2 μsec/cm accommodated the delay time errors, but dispersion in the final data doubled due to the reduced scale of the pictures. Addition of more sophisticated delay and trigger circuits may permit faster sweep rates, but may also introduce new errors in the time measurements.

---

[1] The traverse time of the shock itself for 200 mm is repeatable within 0. 5 μsec; see Appendix B.

3. Data Reduction

The traces shown in Figure 9 were reduced to numerical data using the techniques indicated in the sketches of Figure 10. This is a simple graphical method; optical instruments were not used.

Duff's technique (Ref. 3) is used to obtain curvature measurements. The shock velocity (U_s) one tube diameter upstream of the end plate is used to convert the time measurements to a distance. The time mark (τ_o^i) on each trace ($i = 0, 1, \ldots 4$) is noted first. A line is drawn through each baseline, and another line is drawn through each rising trace with the maximum possible slope. The intercept of these two lines is taken as the shock arrival time at that station (τ_s^i). The shock curvature x^i, parallel to the tube axis, is then determined for the ith station on the end plate diameter, at the instant the shock struck the transducer on the tube axis (τ_s^o) by the relation

$$x^i = U_s \left\{ (\tau_s^i - \tau_s^o) + (\tau_o^o - \tau_o^i) \right\}$$

For thickness measurements, the maximum slope noted above is used again. In this case, the intercepts (τ_b) and (τ_c) of the maximum slope line with the trace are noted along with the shock arrival time (τ_s). Then the maximum slope shock thickness δ_s is determined by

$$\delta_s = U_s \left\{ \tau_b + \tau_c - 2\tau_s \right\}$$

The above approach is necessary because of the difficulty of finding the precise point where maximum slope occurs in a fairly thick trace.

Time can be read from the oscilloscope pictures to an accuracy of 0.05 μsec. This is a relative error of about 5 per cent for measurements halfway between the tube axis and the walls.

It is interesting to note that the traces of Figure 9 do not all show a uniform slope. In fact, the instruments farther away from the tube axis generally show a "thicker" shock than those closer to the center. Qualitatively, one might expect some thickening very close to the sidewalls, but most of the effect observed can be explained by noting that the shock is curved enough to make it strike the faces of the outermost transducers at a small angle; thus it appears to rise a bit slower.

As initial pressure is increased in this series of shots, the traces obtained fall into three categories. At the lowest p_1's, the rising traces are symmetric. As p_1 is increased, the traces are definitely asymmetric (Figure 9c) and the maximum slope is obtained well short of halfway up the rising signal. As the shock rise time approaches the limiting response time of the transducers, a discontinuity appears in the signal separating the maximum slope portion from the remainder of the trace. It is not clear whether the asymmetry of the second and third categories is properly attributed to the precise mechanism of shock reflection rather than a response characteristic of the transducers. The discontinuity of the third category is certainly a transducer characteristic (see Section I, part 4).

In any event, only maximum slope is used to obtain shock thickness, and reasonable results are obtained up to the limiting response speed of the transducers.

At the lowest initial pressures, counter readings indicated that the shock was still accelerating at the time it struck the end plate. As initial pressure was increased, the point of maximum velocity moves upstream from the end plate. Shock attenuation was small enough to neglect in the data reduction, and the velocity used for data reduction is that obtained one tube diameter upstream.

4. Preliminary Results

Sufficient data have been obtained to date to identify some of the parameters influencing shock curvature, and some trends have been tentatively established. The precise functional behavior of the various parameters is not yet completely determined, and it is quite certain that further experimental work will be necessary before a completely valid theory for shock curvature can be written.

The shock shapes obtained (Figure 11) appear to be more parabolic than spherical; if one writes tentatively, using the coordinates indicated in the inset of Figure 11

$$\frac{x}{R} = \text{const.} \left(\frac{r}{R}\right)^n \qquad (1)$$

then it appears that the exponent n has a value between 2.5 and 3.

The scatter is larger in data near the center, especially as p_1 reaches low values. This is partly due to the data reduction process, since a given absolute error in time measurements is a larger relative error where the axial displacement of the shock is small.

It appears, however, that there is also some instability in the shock itself at the lower initial pressures, since the measurements obtained near the tube axis are scattered in a random fashion to a slightly larger extent than the data reduction uncertainty alone would predict. The two symmetrically located instruments give similar readings for a given run but may disagree quite badly with readings obtained on another run at the same conditions. The presence of "tilt" is hence not confirmed, but there may be more truth than poetry in

Duff's observation that the shock "remembers some of the details of its birth at a bursting diaphragm".

The data used in plotting total shock bulge (Figure 12) were obtained by multiplying readings at the instrument nearest the tube wall by 1.28, a number empirically determined by the curves of Figure 11. The empirical formulas obtained by Duff (Ref. 3)

$$x_w = 0.84 \sqrt{\lambda_o R} \tag{2}$$

for his work in the 1.5 inch shock tube in argon, and by Lin (Ref. 4)

$$x_w = 0.5 \sqrt{\lambda_o R} \tag{3}$$

for air in a 24 inch shock tube, where λ_o is the viscosity mean free path and R is the appropriate tube radius, are plotted for comparison. It was found convenient to reduce the above formulas to the form

$$\frac{x_w}{D} = \frac{x_w}{2R} = \text{const.} \sqrt{\frac{\lambda_o}{R}} = \frac{\text{const.}}{\sqrt{Re_w}} \tag{4}$$

where Re_w is a Reynolds number, defined at the wall of the tube by

$$Re_w = \frac{\rho_w u_w D}{\mu_w} \tag{5}$$

or, making the following approximations

$$T_w = T_1 \qquad p_w = p_2$$
$$u_w = u_2 \qquad \rho_w = \rho_2 \frac{T_2}{T_1} \tag{6}$$

Re_w is given in terms of the initial pressure p_1 by

$$Re_w = \gamma M_s \frac{T_2}{T_1} \frac{p_1 D}{\mu_1 a_1} \tag{7}$$

where the subscript $()_2$ refers to conditions behind the shock and the temperature jump T_2/T_1 is given by the ideal gas shock relations using the strong shock approximation (and is quadratic in shock Mach number M_s)[1].

A brief series of runs was made in nitrogen to check the effect of the specific heat ratio γ, and these results are also plotted in Figure 12. It turns out that for Reynolds numbers above 5×10^4, the total shock bulge measurements obtained by Duff and by Lin, as well as those obtained in this investigation, are well represented by the empirical formula[2]

$$\frac{x_w}{D} = \frac{10(\gamma - 1)}{\sqrt{Re_w}} \tag{8}$$

---

[1] Duff's data were converted for Figure 12 using $M_s = 6.3$; for Lin, $M_s = 17$ was taken.

[2] This result has generated some interesting theoretical speculation which will be reported at a later date.

It should be noted that the dependence on Mach number implicit in the definition of Re_w (Eq. 7) has not been checked in this series of experiments. It may just be fortuitous that the arbitrarily assumed average Mach numbers used to re-plot the data of Lin and Duff generate the surprising coincidence indicated in Figure 12.

The dependence on $(\gamma - 1)$ is clearly indicated, and in fact this much can be deduced from a relatively simple calculation. An equation relating the angle β of an oblique shock with the angle θ through which the flow is turned is (Ref. 23, page 88)

$$M_s^2 \sin^2 \beta - 1 = \frac{\gamma + 1}{2} \frac{\sin \theta}{\cos (\beta - \theta)} \tag{9}$$

Making the strong shock approximation, this becomes

$$\sin \beta = \frac{\gamma + 1}{2} \frac{\sin \theta}{\cos (\beta - \theta)} \tag{10}$$

Now (see inset) $\beta = \frac{\pi}{2} - \epsilon$, and ϵ and θ are small angles. Hence

$\sin \theta \doteq \theta$

$\sin \epsilon \doteq \tan \epsilon \doteq \epsilon$

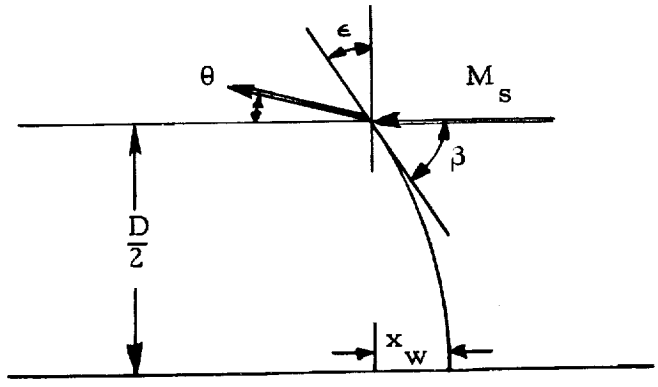

Using the appropriate trigonometric identities, we obtain

$$\epsilon \doteq \frac{\gamma - 1}{2} \theta \tag{11}$$

Assuming the shock is spherical, it can be shown immediately that

$$\tan \epsilon = \frac{(\frac{D}{2}) x_w}{(\frac{D}{2})^2 - x_w^2} \tag{12}$$

hence

$$\epsilon \doteq \frac{2x_w}{D} \doteq \frac{\gamma - 1}{2} \theta \tag{13}$$

relating the total shock bulge to both the specific heat ratio of the gas and the angle through which the flow is turned. Note that the constants selected by Lin and Duff in Equations 2 and 3 have the ratio

$$\frac{0.84}{0.5} = \frac{0.67}{0.4} = \frac{(\gamma - 1)\ \text{argon}}{(\gamma - 1)\ \text{air}} \tag{14}$$

Referring again to Figure 12, it will be noticed that the data obtained at Reynolds numbers below 5×10^4 fall consistently below the empirical line. References 3 and 4 show the same behavior at low Reynolds numbers, though in Duff's case the transition occurs about an order of magnitude lower in Reynolds number than in the larger tubes.

It is interesting and perhaps significant to note that this transition occurs at the same p_1 (in the 17-inch tube) below which the shock is observed to accelerate all the way to the end plate, and that the scatter in measurements taken near the tube axis gets worse at

about the same pressure. Reference 1 indicates that if the tube is long enough, an asymptotic condition will be reached where the separation between the shock and the contact surface becomes constant. It is possible that this condition is characterized by a decelerating shock, and thus that the shock has not reached a stable configuration until it has finished accelerating.

One might thus state, crudely, that if the shock tube is long enough to obtain a decelerating shock at the desired p_1 and Mach number, then its curvature will be given by Equation 8. We note in passing that Duff's small diameter tube has a (length/diameter) ratio almost four times that of the GALCIT instrument. Finally, from the optical instrument maker's point of view, Figure 12 indicates that this crude estimate of shock bulge is at least conservative at the Reynolds numbers where it is no longer accurate.

From the $(\gamma - 1)$ effect one concludes that a shock in a diatomic gas is about fifty per cent less curved, all other conditions being the same, than that obtained in a monatomic gas.

There is a disappointing scatter in the data obtained for shock thickness (Figure 13). It is felt that much of this is in the data reduction process, since the relatively thick traces tend to make location of a precise point of maximum slope quite difficult. A little bit of the dispersion might come from the same shock instability suggested above at the lower p_1's.

Qualitatively at least, shock thickness is observed to vary inversely with p_1, and it is interesting to note that at one pressure the mean of the data obtained agrees exactly with the thickness predicted by reference 1.

REFERENCES

1. Liepmann, H. W.; Roshko, A.; Coles D.; and Sturtevant, B.: A 17 Inch Diameter Shock Tube for Studies in Rarefied Gas Dynamics. Review of Scientific Instruments (June 1962).

2. Hartunian, R. A.: Shock Curvature due to Boundary Layer Effects in a Shock Tube. Physics of Fluids, Vol. 4, p. 1059 (September 1961).

3. Duff, R. A.: Shock Wave Curvature at Low Initial Pressure. Physics of Fluids, Vol. 4, p. 812 (July 1961).

4. Lin, S. C.: Low Density Shock Tube for Chemical Kinetics Studies. Physics of Fluids, Vol. 4, p. 238 (February 1961).

5. Giannini Controls Corporation: Pressure Transducing and Instrumentation Techniques. (2 volumes) WADD TR 59-743 (1 August 1960).

6. Lion, K. S.: Instrumentation in Scientific Research. McGraw-Hill Book Company, New York (1959).

7. Mason, W. P.: Physical Acoustics and Properties of Solids. D. Van Nostrand Company, New York (1958).

8. Mason, W. P.: Piezoelectric Crystals and their Application to Ultrasonics. D. Van Nostrand Company, New York (1950).

9. Mason, W. P.: Electromechanical Transducers and Wave Filters. D. Van Nostrand Company, New York (1948).

10. von Hippel, A. R. (editor): Dielectrics and Waves. Massachusetts Institute of Technology, Technology Press (John Wiley and Sons), New York (1954).

11. von Hippel, A. R. (editor): Dielectric Materials and Applications. Massachusetts Institute of Technology, Technology Press (John Wiley and Sons), New York (1954).

12. von Hippel, A. R. (editor): Molecular Science and Molecular Engineering. Massachusetts Institute of Technology, Technology Press (John Wiley and Sons), New York (1959).

13. Hueter, T. F.; and Bolt, R. H.: Sonics. John Wiley and Sons, New York (1955).

14. Redwood, M.: Transient Performance of a Piezoelectric Transducer. Journal of the Acoustic Society of America, Vol. 33, p. 527 (April 1961).

15. Jaffe, B.: A Primer on Ferroelectricity and Piezoelectric Ceramics. Clevite Engineering Memorandum 60-14, Electronic Research Division, Clevite Corporation, Cleveland, Ohio (December 1960).

16. Jaffe, H. (chairman): IRE Standards on Piezoelectric Crystals: Measurements of Piezoelectric Ceramics, 1961. Proceedings of the Institute of Radio Engineers, Vol. 49, p. 1161 (July 1961).

17. Posel, K.: The Recording of Pressure Step Functions of Low Amplitude by means of a Composite-Dielectric Capacitance Transducer placed in a Parallel-T Network. Department of Mechanical Engineering, Report 1/61, University of the Witwaterstrand, Johannesburg (January 1961).

18. Willmarth, W. W.: A Small Barium Titanate Transducer for Aerodynamic or Acoustic Pressure Measurements. Review of Scientific Instruments, Vol. 29, p. 218 (March 1958).

19. Farrand, W. B.: Piezoelectric Pressure Sensing Devices. Poulter Laboratories TR 010-60, Stanford Research Institute (July 1960).

20. Zaitsev, S. G.: Measurement of Rapidly Varying Pressures in a Gas. Instruments and Experimental Techniques (Pribory i Tekhnika Eksperimenta,) p. 811 (1958).

21. Makushkin, V. P.; and Mishuyev, A. V.: Spherical Barium Titanate Receivers for Measuring the Pressure of Shock Waves in Air. Soviet Physics: Acoustics, Vol. 5, p. 64 (1959).

22. Sinnott, M. J.: The Solid State for Engineers. John Wiley and Sons, New York (1958).

23. Liepmann, H. W.; and Roshko, A.: Elements of Gasdynamics. John Wiley and Sons, New York (1957).

24. Kolsky, H.: Stress Waves in Solids. Clarendon Press (1953).

25. Miklowitz, J.: The Propagation of Compressional Waves in a Dispersive Elastic Rod. Journal of Applied Mechanics, Vol. 24, p. 231 (February 1957).

26. Miklowitz, J.; and Nisewanger, C. R.: The Propagation of Compressional Waves in a Dispersive Elastic Rod. Journal of Applied Mechanics, Vol. 24, p. 240 (February 1957).

27. Feldman, S.: Hypersonic Gas Dynamic Charts for Equilibrium Air. AVCO Research Laboratory, AVCO Corporation (January 1957).

APPENDIX A

TRANSIENT PERFORMANCE OF A PIEZOELECTRIC TRANSDUCER

I. General Piezoelectric Equations

The most general piezoelectric equations for the receiver application are, in Cartesian tensor notation,

$$T_{mn} = c^{D}_{mnij} S_{ij} - h_{kmn} D_k \tag{1}$$

$$E_i = - h_{imn} S_{mn} + \beta^{S}_{ik} D_k \tag{2}$$

where all subscripts range from 1 to 3, and

T_{mn} = elastic stress tensor

S_{mn} = elastic strain tensor

c^{D}_{mnij} = elastic constants at constant electric displacement

β^{S}_{ik} = dielectric impermeability at constant strain

h_{kmn} = piezoelectric "stiffness" constants

E_i = electric field vector

D_k = electric displacement vector

The usual symmetry of the stress and strain tensors permits use of a reduced tensor notation, in which the two stress/strain subscripts are replaced with a single index ranging from 1 to 6. Equations 1 and 2 above then become

$$T_m = c^D_{mn} S_n - h_{km} D_k \qquad (1a)$$

$$E_i = -h_{im} S_m + \frac{1}{\epsilon} D_i \qquad (2a)$$

$(i,j,k = 1,2,3; \quad m,n = 1,2, \ldots 6)$ where $\epsilon = \frac{1}{\beta}$, the dielectric constant of the material, is usually assumed to be constant in all directions. Note that where the reduced elastic tensor notation is used, $h_{ij} \neq h_{ji}$, since the first subscript ranges from 1 to 3 and represents the electric direction while the second subscript ranges from 1 to 6 and represents both normal (1 to 3) and shear (4 to 6) "directions".

The appendix of Mason's most recent text (Ref. 7) is an almost exhaustive derivation of all the various interrelationships between mechanical, electrical, thermal, magnetic and other properties of materials from thermodynamic potentials. The work is done in Cartesian tensors and makes most interesting and profitable reading, if only for its completeness.

The Institute of Radio Engineers (Ref. 16) has recently published a standard for the piezoelectric notation. The paper includes a description of the experimental processes to be used in the determination of the various constants for a material. The reduced elastic tensor notation is used, and all quantities are reported in the rationalized MKSC system of units. The manufacturers of piezoceramic materials have generally accepted this notation for their catalogs.

The manufacturers usually report piezoelectric constants d_{im} or g_{im} instead of the more useful h_{im}. Conversion can be accomplished with the formulas

$$h_{im} = \beta^{S}_{ik} c^{E}_{mn} d_{kn} = c^{E}_{mn} g_{in} \tag{3}$$

where i,k range from 1 to 3 (electric)

m,n range from 1 to 6 (elastic)

II. Transient Performance Equations

Using a one-dimensional analysis and the Laplace transform

$$\mathcal{L} f(t) = \bar{f}(p) = \int_{o}^{\infty} \exp(-pt) f(t) dt \tag{4}$$

Redwood (Ref. 14) obtains the following five equations governing the transient performance of a piezoelectric thin plate bonded to two infinite media (see figure):

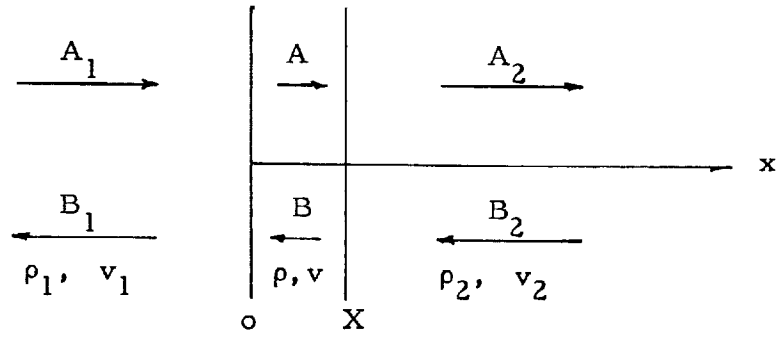

For the displacement $(\bar{\xi})$ in each of the three media (subscripts are omitted):

$$\bar{\xi} = A \exp\left(-\frac{px}{v}\right) + B \exp\left(+\frac{px}{v}\right) \tag{5}$$

For the force $(\bar{F})$ in the non-piezoelectric components (subscripts 1, 2)

$$\bar{F} = pZ \left\{ - A \exp\left(- \frac{px}{v}\right) + B \exp\left(+ \frac{px}{v}\right) \right\} \tag{6}$$

where Z is the mechanical impedance of the element; specifically, using the material density ρ, the wave speed v, and a cross-sectional area S,

$$Z = \rho v S \tag{7}$$

For the electromechanical equilibrium of the piezoelectric element (no subscript)

$$\bar{F} + h\bar{Q} = pZ \left\{ - A \exp\left(- \frac{px}{v}\right) + B \exp\left(\frac{px}{v}\right) \right\} \tag{8}$$

where $\bar{Q}$ is the charge on the element, h is a piezoelectric constant. Finally, the voltage output $(\bar{V})$ of the element is

$$\bar{V} = - h \left\{ (\bar{\xi})_X - (\bar{\xi})_o \right\} + \frac{\bar{Q}}{C_o} \tag{9}$$

where $(\bar{\xi})_X$ and $(\bar{\xi})_o$ are the displacements of the faces $x = X$ and $x = 0$ and C_o is the static capacitance of the piezoelectric element.

In the above equations, A and B (with appropriate subscripts) are eliminated by use of the boundary conditions

$$\begin{aligned} (\bar{\xi}_1)_o &= (\bar{\xi})_o; & (\bar{\xi})_X &= (\bar{\xi}_2)_X; \\ (\bar{F}_1)_o &= (\bar{F})_o; & (\bar{F})_X &= (\bar{F}_2)_X \end{aligned} \tag{10}$$

It can also be assumed that the materials (1) and (2) are infinitely long, hence $B_2 = 0$. In the general case, one must also know the electrical characteristics of the circuit in which the piezoelectric element is connected. It will be assumed here that the element is loaded with a resistive load (R) only. Then Ohm's law gives

$$\bar{V} = -\bar{I}R = -p\bar{Q}R \tag{11}$$

where the minus sign arises because the current $I = dQ/dt$ is defined positive for $+Q$ increasing, but the current through a resistor is positive when flowing to a point of lower potential.

Now at $x = 0$, using Equations 2, 3, and 4 with the boundary conditions

$$(\bar{\xi}_1)_o = (\bar{\xi})_o = A_1 + B_1 = A + B \tag{12}$$

$$(\bar{F}_1)_o = (\bar{F})_o = pZ_1(-A_1 + B_1) = pZ(-A + B) + \frac{h\bar{V}}{p^2R} \tag{13}$$

Combining,

$$2A_1Z_1 = A(Z + Z_1) - B(Z - Z_1) - \frac{h\bar{V}}{p^2R} \tag{14}$$

or

$$A - r_oB = A_1(1 - r_o) + \frac{h\bar{V}(1 + r_o)}{2p^2RZ} \tag{15}$$

where

$$r_o = \frac{Z - Z_1}{Z + Z_1} \tag{16}$$

Similarly, at $x = X$ the charge is $-Q$ and

$$(\bar{\xi})_X = (\bar{\xi}_2)_X = Ae^{-p\tau} + Be^{+p\tau} = A_2 e^{-p\tau} \tag{17}$$

$$(\bar{F})_X = (\bar{F}_2)_X = pZ(-Ae^{-p\tau} + Be^{+p\tau}) - \frac{h\bar{V}}{p^2 R} = -pZ_2 A_2 e^{-p\tau} \tag{18}$$

Combining as before,

$$r_x A + Be^{2p\tau} = \frac{hV(1-r_x)e^{p\tau}}{2p^2 RZ} \tag{19}$$

where

$$r_x = \frac{Z_2 - Z}{Z_2 + Z}; \qquad \tau = \frac{X}{v} \tag{20}$$

Finally, from Equation 6,

$$\bar{V}(1 + \frac{1}{pC_o R}) = -h(Ae^{-p\tau} + Be^{+p\tau}) + h(A + B) \tag{21}$$

or

$$\bar{V}(1 + \frac{1}{pC_o R}) = hA(1 - e^{-p\tau}) + hB(1 - e^{+p\tau}) \tag{22}$$

Formally, Equations 15, 19, and 22 can be combined to eliminate A and B, arriving at the general statement of $\bar{V}$ as a function of the input waveform A_1, the piezoelectric constant h, the reflection coefficients r_o and r_x, the transducer rise time τ, and circuit time constants involving R and C_o. It is algebraically much simpler, however, to insert special conditions at this point.

Case 1: Infinite Input Impedance

For the case where R is infinite, much simplification results. Equation 15 becomes

$$A - r_o B = A_1(1 - r_o) \tag{23}$$

Equation 19 becomes

$$r_x A = - Be^{2p\tau} \tag{24}$$

from which, eliminating B

$$A = A_1 \frac{(1 - r_o)}{(1 + r_o r_x e^{-2p\tau})} \tag{25}$$

and Equation 22 gives

$$\bar{V} = \frac{A_1 h(1 - r_o)\left\{ 1 - (1 - r_x)e^{-p\tau} - r_x e^{-2p\tau} \right\}}{(1 + r_o r_x e^{-2p\tau})} \tag{26}$$

Expansion of the denominator by the binomial theorem gives

$$\bar{V} = A_1 h(1 - r_o)\left\{ 1 - (1 + r_x)e^{-p\tau} + r_x(1 + r_o)e^{-2p\tau} + \ldots \right\} \tag{27}$$

Now the expression inside the brackets transforms with the relation

$$\mathcal{L} f(t - \tau) = e^{-p\tau}\left\{ \mathcal{L} f(t) \right\} \tag{28}$$

thus the series inside the brackets of Equation 27 gives a damped ringing function, with period the same as the rise time of the transducer. In the special case $r_x = 0$, the series collapses and

$$\bar{V} = A_1 h(1 - r_o)(1 - e^{-p\tau}) \tag{29}$$

If a step function of force is applied

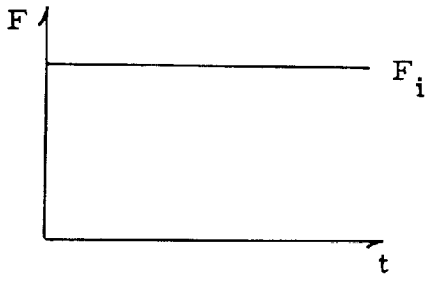

$$F = 0, \quad t < 0$$

$$F = F_i, \quad t > 0$$

$$\bar{F}(p) = \frac{F_i}{p}$$

Equation 6 gives at $x = 0$

$$F_i = p^2 Z_1(-A_1); \qquad A_1 = -\frac{F_i}{p^2 Z_1} \tag{30}$$

and transforming Equation 29, the result is

$$V(t) = -\frac{hF_i(1 - r_o)}{Z_1}\left\{t - (t - \tau)\right\} \tag{31}$$

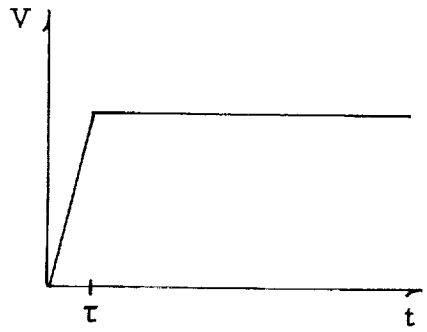

Case 2: Finite Input Impedance, Matched Backing

In practice, R is finite. However, it frequently occurs that the reflection coefficient r_x is nearly zero; that is, that an impedance match has been obtained on the back face of the crystal. In this case, Equation 15 is unchanged. Equation 19 becomes

$$B = \frac{h\bar{V}e^{-p\tau}}{2p^2FZ} \tag{32}$$

Substitution into Equations 12 and 19 gives

$$A = A_1(1 - r_o) + \frac{h\bar{V}}{2p^2RZ}\left\{1 + r_o(1 + e^{-p\tau})\right\} \tag{33}$$

$$\bar{V} = \frac{hp^2A_1(1-r_o)(1-e^{-p\tau})}{(p+\alpha)(p+\beta) + \frac{h^2r_oe^{-p\tau}}{2RZ}} \tag{34}$$

This will be recognized as equivalent to Equation 29 except for the time constants α and β, which are the roots of

$$p^2 + \frac{p}{C_oR} - \frac{h^2r_o}{2RZ} = 0 \tag{35}$$

or

$$\alpha = -\frac{1}{2C_oR} + \left\{\frac{1}{(2C_oR)^2} + \frac{h^2r_o}{2RZ}\right\}^{1/2}$$

$$\beta = -\frac{1}{2C_oR} - \left\{\frac{1}{(2C_oR)^2} + \frac{h^2r_o}{2RZ}\right\}^{1/2} \qquad (36)$$

After binomial expansion of the denominator, Equation 34 has the form

$$V = \frac{hp^2A_1(1 - r_o)}{(p + \alpha)(p + \beta)} \sum_{n=o}^{\infty} \gamma^n(e^{-2np\tau} - e^{-(2n+1)p\tau}) \qquad (37)$$

where $$\gamma = \frac{\alpha\beta}{(p + \alpha)(p + \beta)} \qquad (38)$$

For a step function input, the term multiplying the series is, when transformed,

$$-\frac{hF_i}{Z}(1 + r_o)\left\{\frac{e^{-\alpha t} - e^{-\beta t}}{\beta - \alpha}\right\} \qquad (39)$$

Depending on the relative magnitude of the terms in Equation 36, this expression may either grow or decay very rapidly. Since $\alpha = A + B$, $\beta = A - B$, the expression (39) has the form

$$-\frac{hF_i}{Z}(1 + r_o)e^{-At}\sinh Bt. \qquad (40)$$

Case 3: Front and Back Impedance Match

Finally, for the case where both front and back faces of the piezoelectric are matched ($r_o = r_x = 0$), Equations 36 collapse to

$$\alpha = 0, \qquad \text{hence} \qquad \gamma = 0$$

$$\beta = -\frac{1}{C_o R} \tag{41}$$

Equation 34 takes on the much more tractable form

$$\bar{V} = \frac{hpA_1}{p + \beta}\left(1 - e^{-p\tau}\right) \tag{42}$$

which for a step function transforms back to

$$V = + \frac{hF_i RC_o}{Z}\left(1 - e^{-\beta t}\right)\left\{t - (t - \tau)\right\} \tag{43}$$

APPENDIX B

17-INCH SHOCK TUBE CONFIGURATION

The excellent description of the construction and basic configuration of the GALCIT 17-inch shock tube in Reference 1 need not be repeated here. Very briefly, the tube is conventionally driven; the test section (measured from the diaphragm) is 20.70 meters long with a uniform inside diameter of 434 millimeters. Figure 4 schematically suggests the layout.

A set of four mechanical pumps evacuates the test section to approximately 0.002 micron Hg in 30 minutes. The maximum leak rate recorded with all instrumentation installed is 0.05 micron/hour. Static pressure in the test section is measured with a battery of pressure gages (aneroid, Pirani, and McLeod).

An independent mechanical pump evacuates the driver to a few microns, ensuring purity of the driver gas and consequent repeatability of Mach number. Pressure in the driver is measured to an accuracy of 0.5 mm Hg with a group of three aneroid gages, for reasons which will be explained later. A design limit of 15 atmospheres is imposed on the driver to avoid equilibrium over-pressures above one atmosphere on completion of a shot.

Precise diaphragm bursting pressures are achieved with a cruciform knife blade, permitting a highly repeatable shock for a given test section condition. As noted in Reference 1, errors in measurement of test section pressure (p_1) probably account for as much Mach number deviation at a given driver pressure (p_4) as any events transpiring in the driver or at the diaphragm.

An effort to simplify the test gas injection procedure at very low pressures (typically a few microns), while assuring maximum accuracy and repeatability, has led to the development of a unique and very simple system for this purpose. Boyle's law for isothermal expansion of a perfect gas is

$$PV = \text{const.}$$

This is, in the final analysis, the basic calibration technique for all pressure instruments; comparison of pressures in known absolute volumes is the principle of operation of the McLeod gage.

The enormous volume of the shock tube test section (3065 liters) suggested the construction of a chamber with a volume of 3065 milliliters, in which the test gas pressure could easily be measured to an accuracy of 0.5 per cent on a good aneroid instrument in the millimeter range. Then when admitted to the tube, test gas pressure would be the same number of microns with the same accuracy. The great attractiveness of this system is that the cumbersome machinery of needle-valve gas injection by guesswork followed by McLeod gage measurements is completely eliminated.

A schematic sketch of the system described above is presented in Figure 14. The calibrated chamber is a brass cylinder, 100 millimeters in diameter and approximately 370 millimeters long. The volume ratio of the shock tube to the chamber itself is actually about 997 to 1, since the simple statement of Boyle's law indicated above must be written

$$P_c V_c = P_t(V_c + V_t + V_p)$$

where the subscript $()_c$ refers to the initial condition in the calibrated chamber, $()_t$ refers to the final condition in the shock tube, and V_p is the volume of the plumbing between chamber and tube (in this case about three times the volume of the chamber itself). It should be noted that the volume of the aneroid gage connected to the chamber is quite large and is included in the chamber volume.

The system is calibrated against the McLeod gage installed on the shock tube. The volume was originally about ten per cent too large; it was brought down to the correct size by insertion of about 150 steel ball bearings, $\frac{1}{2}$ inch diameter. If future changes of the shock tube dimensions are contemplated, the chamber volume may be adjusted by adding or removing the balls.

The 17-inch shock tube as presently operating can thus repeat Mach numbers to greater accuracy than the ability of installed microsecond counters to record them (about 0.5 per cent)[1]. In fact, counter readings can be predicted to 1 per cent before a shot, given the driver and test gases and their respective pressures and the room temperature, from the basic shock tube performance equation

$$\frac{P_4}{P_1} = \frac{1 + \frac{2\gamma_1}{\gamma_1+1}(M_s^2 - 1)}{\left\{1 - \frac{\gamma_4 - 1}{\gamma_1 + 1}\,\frac{a_1}{a_4}\,\frac{M_s^2 - 1}{M_s}\right\}^{\frac{2\gamma_4}{\gamma_4 - 1}}}$$

[1] For example, rms Mach number deviation from a nominal 7.68 over 16 runs at $p_4 = 25$ psig, $p_1 = 60\ \mu$ was $\pm$ 0.4 per cent. A room temperature change of $\pm$ 5°C, if unnoticed, will cause almost $\pm$ 0.9 per cent scatter.

whether or not any previous runs have been made under these particular conditions. The advantage from a purely economic point of view is obvious.

Current operation of the driver is also of some interest. While knife blades give excellent repeatability of bursting pressure, a given diaphragm material and thickness is useful only over a limited pressure range. The lower limit is typically about 70 per cent of the free bursting pressure. The upper limit is presently somewhat less than the free bursting pressure due to the loss of petals from the action of the reflecting shock. While most of these are torn loose and come to rest in the driver, some chunks of aluminum the size of a saucer have flown the length of the test section and struck the end plate.

Pending modification of the knife blades and testing of new diaphragm materials, the driver pressure range is thus considerably restricted (an 0.020 inch aluminum diaphragm, for example, covers the range from 18 to 25 psig -- above this it sheds petals).

There are, however, some advantages to working at a fixed, low driver pressure. As noted in Section I, the "galloping zero" typical of pressure transducers sensing stresses in the tube wall is directly related to p_4. There is less chance for operator error in knife blade settings if the blades are left alone. Finally, operating costs are directly related to driver pressure -- six high pressure helium bottles are exhausted by about 20 shots at 20 psig.

A glance at the basic shock tube performance equation shows that as p_1 increases, either p_4 or a_4 (or both) must be increased to maintain a constant Mach number. If p_4 is held constant, a_4 may

be increased either by heating the driver or varying the composition of the driver gas. The first solution is rather cumbersome and expensive, though certainly feasible. The second solution is simple and inexpensive.

Driver plumbing is arranged so that two independent high-pressure lines (presently helium and nitrogen) terminate in regulators at the console. Either gas, or both, may be admitted to the driver through throttle valves. With suitable aneroid instruments, partial pressures of as little as 0.02 per cent (of a total pressure of 2000 mm Hg absolute) can be admitted accurately.

In the shock curvature series of shots, the pressure range (p_1) to be covered was 30 to 500 microns in argon. It was decided to keep p_4 constant at 18 psig, using helium as the basic driver gas, with Mach number held as nearly constant as possible. If the shots at the highest p_1 were to be made with pure helium driving into argon, then the driver could be contaminated with nitrogen to suppress the Mach number at the lower p_1, and Mach number could be kept constant by decreasing the partial pressure of nitrogen added as p_1 was increased.

The amount of nitrogen to be used was determined by the lowest possible Mach number giving a suitable pressure step for measurements at a p_1 of 30 microns (see Figure 7a). This turned out to be a Mach number of 7.35, obtained with a 5 per cent N_2 - 95 per cent He mixture.

This manipulation of driver composition turned out to be a highly useful technique. After a few points were obtained, the percentage of nitrogen to be added on further shots was calculated from the curve (and the simple formula) presented in Figure 15. Total Mach number deviation from the desired constant 7.35, from all causes, was less than three per cent.

Obviously other gases will perform in the same manner. In this case, contamination with argon would have been more effective in reducing the Mach number; on the other hand, a gas of intermediate molecular weight (perhaps ammonia, methane or neon) would have permitted the use of larger percentages and avoided the slight inconvenience of measuring a partial pressure of 2 mm in a total of 2000.

APPENDIX C

TRANSDUCER CONTINUITY TEST CIRCUIT

A single shot experiment typical of shock tubes requires close attention to instrumentation. In particular, when large numbers of instruments are used to determine geometric properties of a shock, failure of one of them may result in a complete loss of usable data, hence a wasted shot.

Electrical instruments, especially those under development, are quite prone to failures of one kind or another; and when they are intimately connected to a vacuum system, the problem of checking them all immediately before each shot may be quite difficult and unnecessarily time-consuming.

Thin film heat gages are easily checked for continuity with a simple volt-ohm meter. Any significant change in resistance or voltage drop across the gage is an immediate indication of trouble. The situation is quite different with instruments relying on a capacitance to generate the signal; some sort of AC bridge is then required to assure continuity.

While a number of excellent AC bridges are commercially available, most of them are expensive and their readings, while very accurate, are somewhat difficult to obtain and interpret. The best circuit to obtain a quick check on the condition of a capacitance-dependent instrument should give immediate, unmistakable indications of the following:

1. Open circuit

2. Short circuit

3. Significant change (perhaps 5 per cent) from the known "good" capacitance value.

The very simple system described below meets the above requirements nicely. It should be noted that an inexpensive oscilloscope was readily available here, whereas an impedance bridge was not. Other experimenters may not share this misfortune.

Consider the parametric equations of a plane curve

$$x = A_1 \sin \omega_1 t \qquad (1)$$

$$y = A_2 \sin (\omega_2 t + \theta)$$

Applied to the horizontal and vertical deflection plates respectively of an oscilloscope, the trace described by the above equations is one of the familiar family of Lissajous figures. In particular, when $A_1 = A_2$ and $\omega_1 = \omega_2$, the resulting trace is an ellipse, with orientation and eccentricity determined by the phase angle θ between the two voltages. The special case $\theta = \frac{\pi}{2}$ generates a circle.

The parallel LCR circuit sketched below will, when connected to the vertical (V) and horizontal (H) deflection circuits of an oscilloscope, generate the desired family of ellipses.

$$I_L + I'_L = \frac{V_o}{Z_L} e^{j\omega t} = \frac{V_o e^{j\omega t}}{Z_L^2} (R_L - j\omega L) \qquad (4)$$

and

$$I_C + I'_C = \frac{V_o e^{j\omega t}}{Z_C^2} (R_C + \frac{j}{\omega C}) \qquad (5)$$

Insertion into Equation 3 gives, after cancellation of common factors,

$$R_L R_C = \frac{L}{C} \qquad (6)$$

Now from the circuit sketched,

$$R_L + R_C = 2R \qquad (7)$$

Thus for a circle

$$C = \frac{L}{R^2} \left\{ \frac{1}{2\frac{R_C}{R} - (\frac{R_C}{R})^2} \right\} \qquad (8)$$

Hence if L and R are known, C is determined by the setting of the variable resistance at which a circle is obtained. The most attractive feature of this circuit in continuity checking is that relatively small deviations from the correct value of C for a given $\frac{R_C}{R}$ are immediately apparent in the shape of the figure on the screen. Gross deviations, such as a short or open circuit, are apparent immediately regardless of the setting of $\frac{R_C}{R}$.

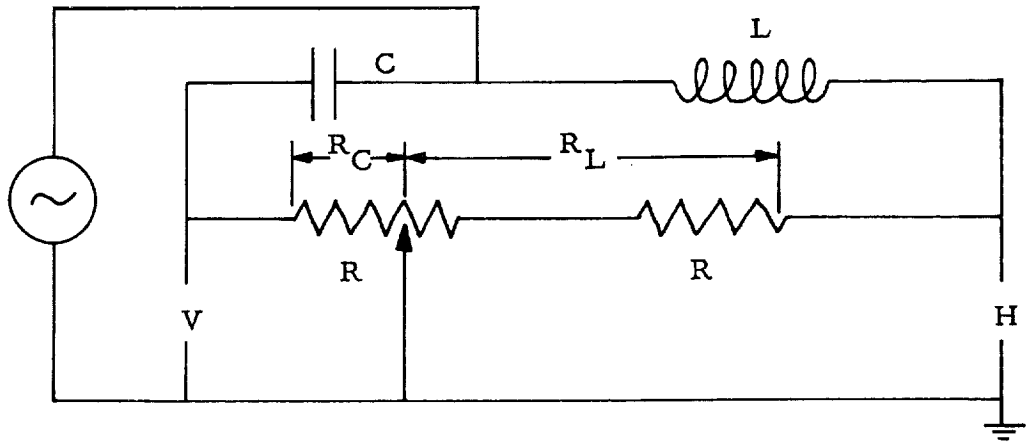

From the vector diagram of currents in the circuit

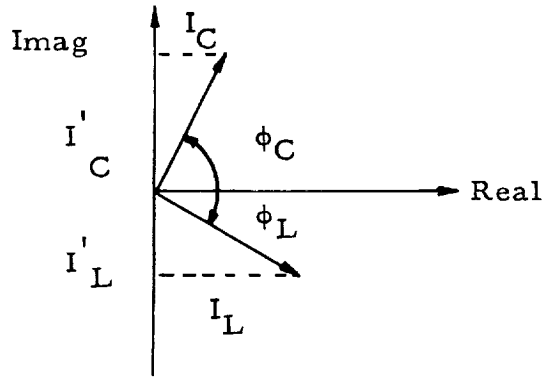

it is evident that the condition for a circular trace is

$$\phi_C - \phi_L = \frac{\pi}{2} \tag{2}$$

This condition is satisfied if

$$\frac{I_C}{I'_C} = \frac{I'_L}{I_L} \tag{3}$$

In the usual complex notation,

In many oscilloscopes, the gain of the horizontal amplifier may be fixed at a fairly low value, while the vertical amplifier may offer a broad range of sensitivity. This condition may be compensated for by adjusting the values of R, L, and the frequency of the signal generator. Suppose a gain of k is desired on the horizontal signal. Then

$$\left| (I_L + I_L')R_L \right| = k \left| (I_C + I_C')\, R_C \right| \tag{9}$$

Inserting the appropriate values, after some algebra

$$k^2 \omega^4 (R_C C)^4 + (k^2 - 1)\omega^2 (R_C C)^2 - 1 = 0 \tag{10}$$

with the solution

$$k = \frac{1}{\omega R_C C} \tag{11}$$

or alternatively

$$k = \frac{R_L}{\omega L} \tag{12}$$

If $\frac{R_C}{R} = 0.5$, R is 1000 ohms, C is about 10^{-9} farad and a gain of 10 is desired, a frequency of about 30 kilocycles and an inductance of about 0.75×10^{-3} henry should be chosen. The circuit is calibrated with a decade capacitor. A plot of Equation 8 is sketched below.

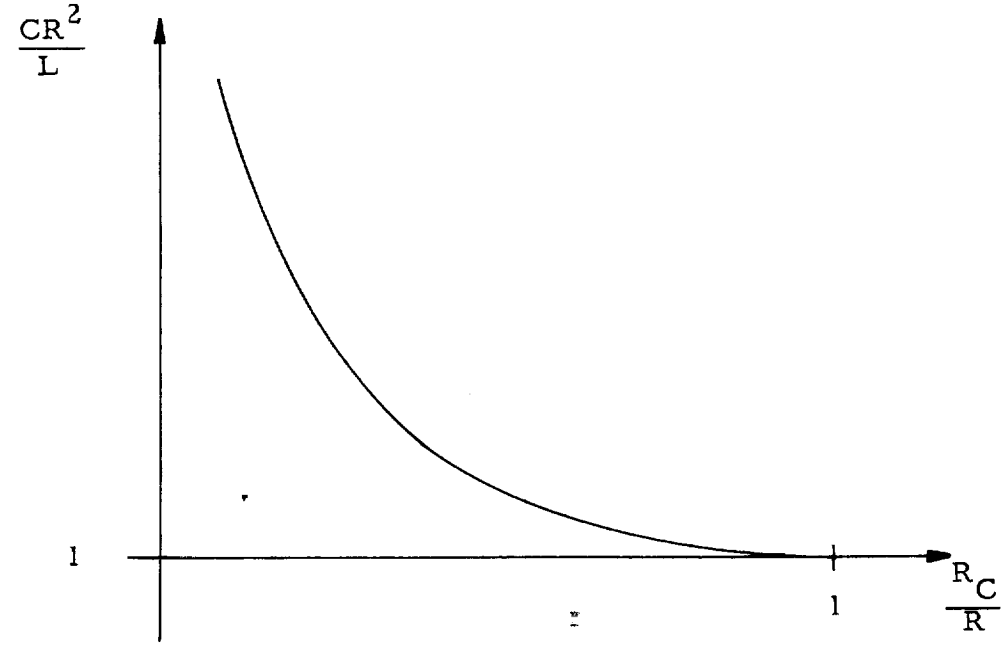

Typical traces obtained with this circuit demonstrate clearly its effectiveness as a quick and reliable method of checking circuit continuity.

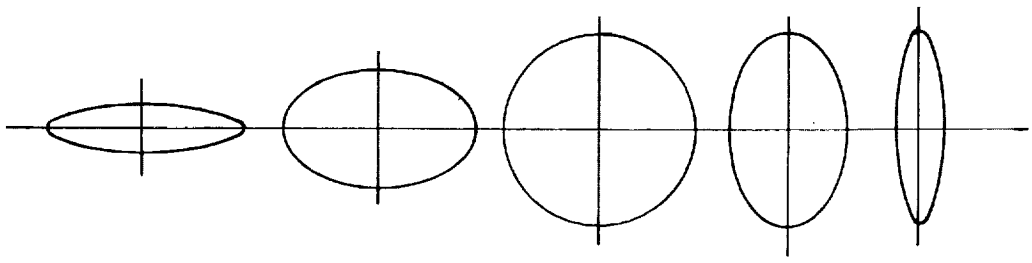

(a) (b) (c) (d) (e)

The cases illustrated are:

(a) Open circuit at transducer; some cable capacitance

(b) Circuit capacitance about 5 per cent low;

(c) Balance ($\frac{R_C}{R}$ is the same as that noted when the transducer was first checked)

(d) Circuit capacitance about 5 per cent high;

(e) Short circuit

TABLE I

SELECTED PIEZOCERAMIC CONSTANTS FOR THIN DISC RECEIVERS*

	k_3	$N_3=\frac{1}{2}\sqrt{\frac{c}{\rho}}$	g_{33}	$h_{33}=g_{33}c$	$Z_3=2\rho N_3$	T_c	ϵ
$BaTiO_3$	0.46	2840	14.0	1.55	31.2	100	1200
PZT-2	0.62	2090	36.8	2.63	32.0		450
PZT-4	0.64	2000	24.0	1.61	30.0	300	1200
PZT-5A	0.675	1890	24.4	1.42	28.4	300	1500
PZT-5B	0.66	1940	19.6	1.28	29.1	300	2000
PZT-6	0.54	2060	17.0	1.21	30.6		1100

k_3 = Longitudinal coupling factor (dimensionless)

N_3 = Frequency constant, disc thickness mode, meters/second

g_{33} = Voltage constant, 10^3 volt meters/newton

h_{33} = Stiffness constant, 10^9 coulombs/newton

Z_3 = Acoustic impedance, 10^6 kilograms/second meter^2

T_c = Curie temperature, ^oC

c = Young's modulus, newton/meter^2

ρ = Density, kilograms/meter^3

ϵ = Dielectric constant referred to free space

*Data furnished by Clevite Corporation

TABLE II

SELECTED PROPERTIES OF METALS

Material	V_{ext}	ρ	$Z_{ext}=V\rho$
Brass	3480	8.6	30.0
Copper	3750	8.6	32.1
Iron, electrolytic	5120	7.7	39.3
Monel metal	4400	8.9	39.1
Silver	2680	10.4	27.9
Stainless steel, no. 347	5000	7.9	39.5
Zinc, rolled	3850	7.1	27.1

Source: Mason, Ref. 7, page 17

V_{ext} = Extensional (rod) velocity, meters/second

ρ = Density, kg/meter^3

Z_{ext} = Specific (rod) impedance, kg/second meter^2

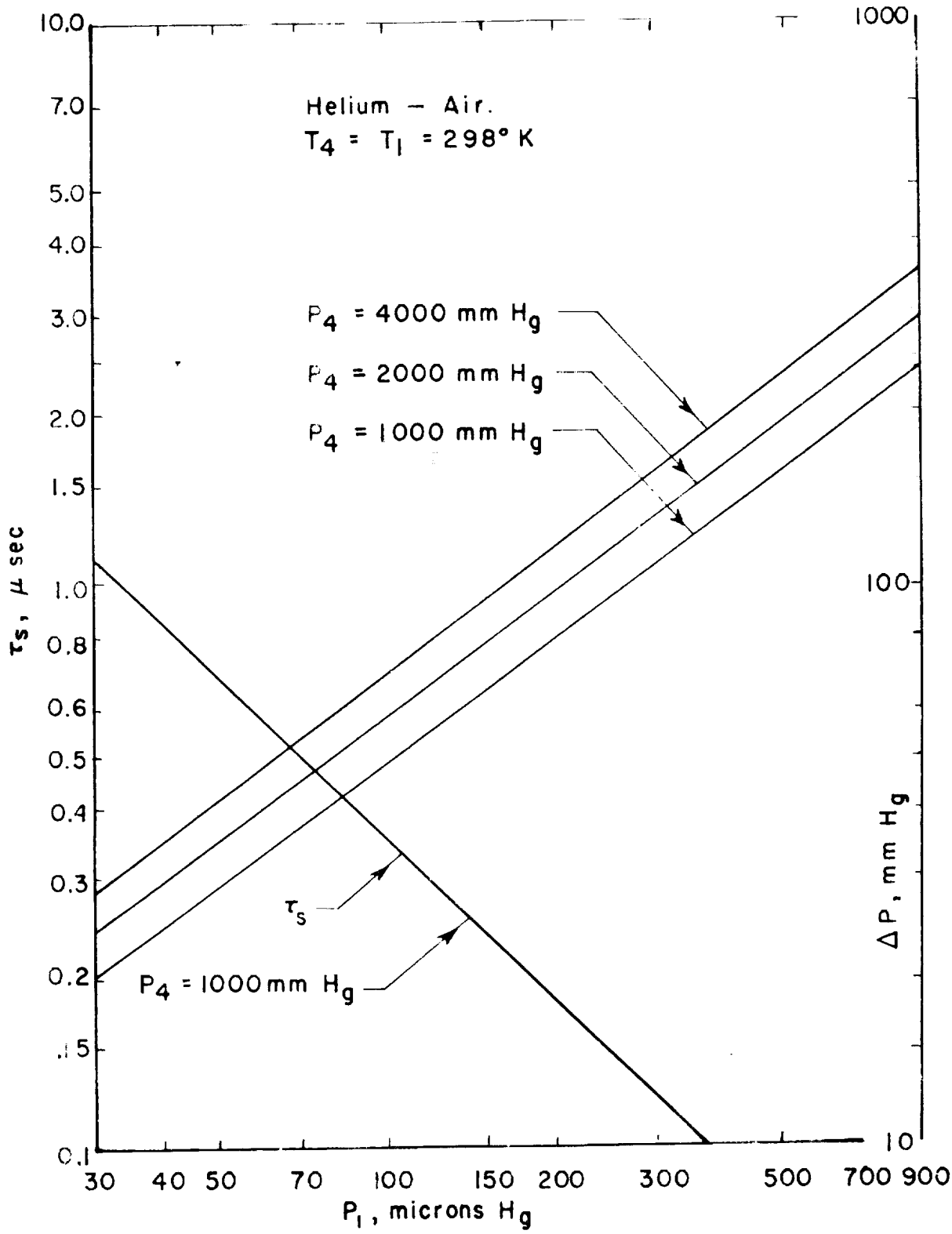

FIG. 1 CALCULATED SHOCK RISE TIME, PRESSURE STEP

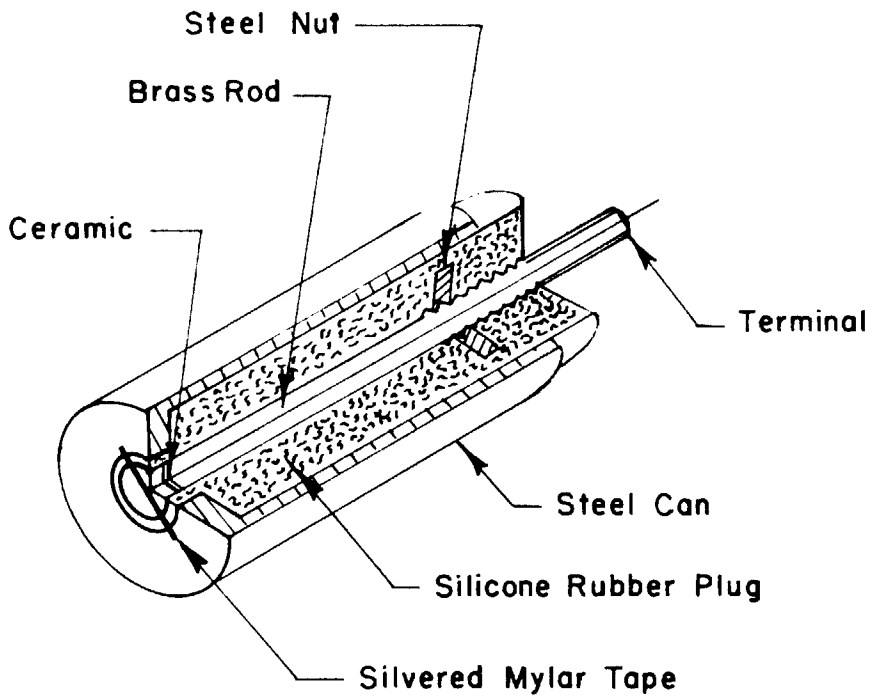

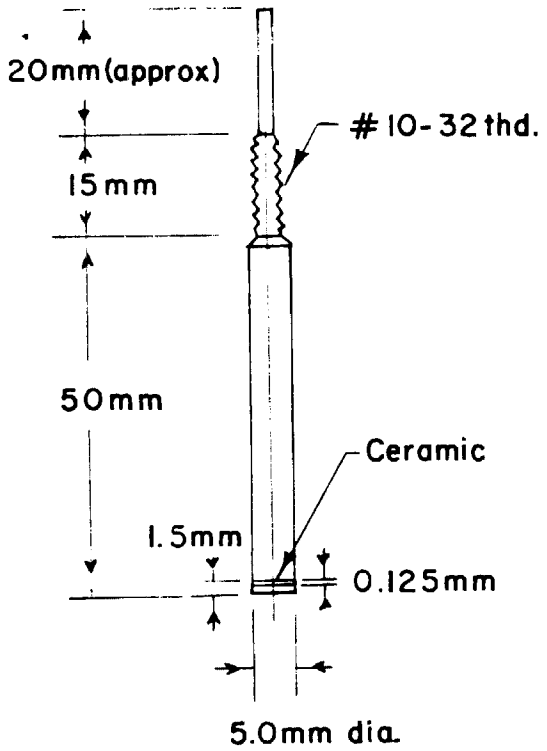

FIG. 2 TRANSDUCER ASSEMBLY AND SENSITIVE ELEMENT

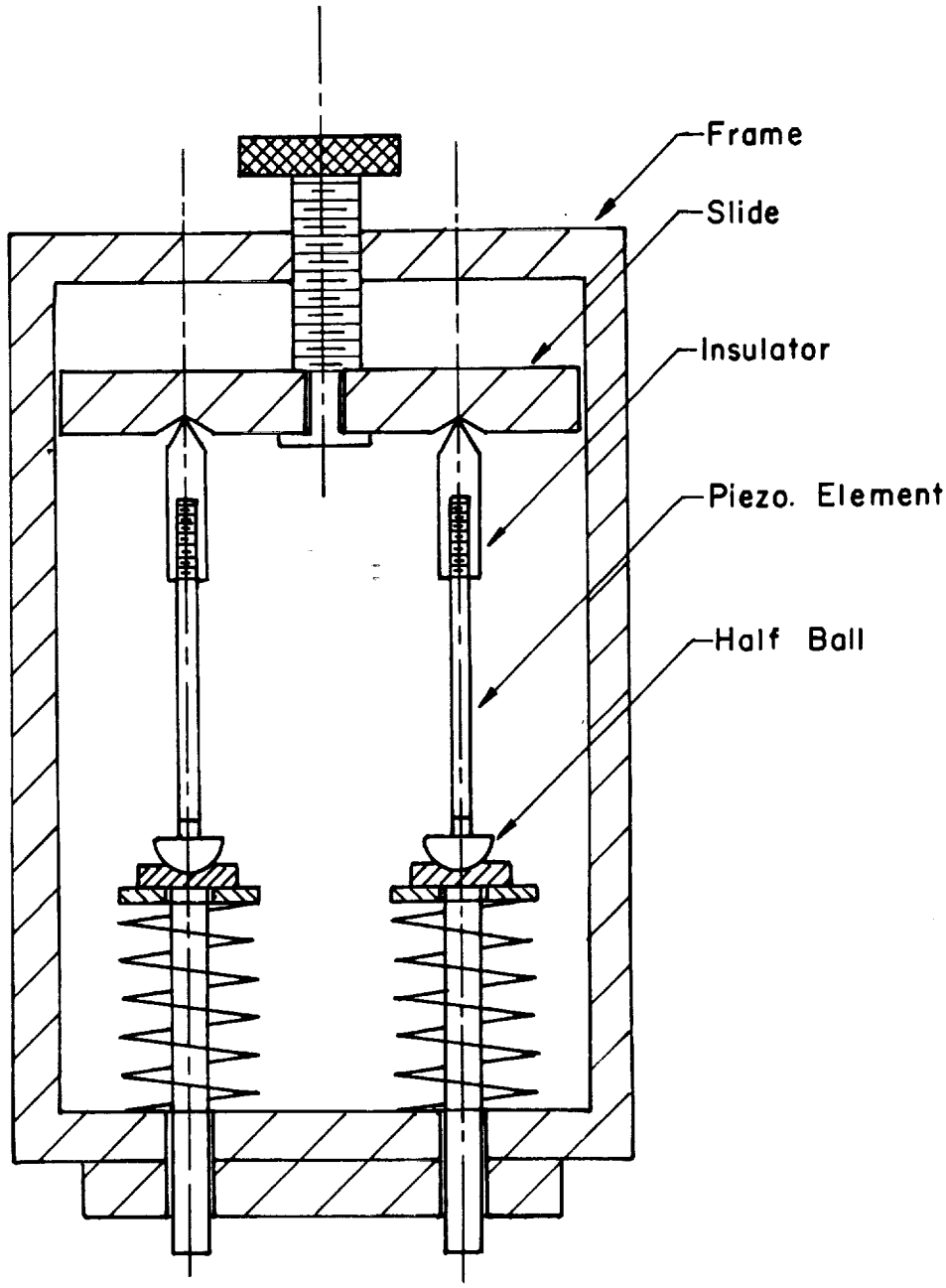

FIG. 3 BONDING/POLARIZATION CLAMP

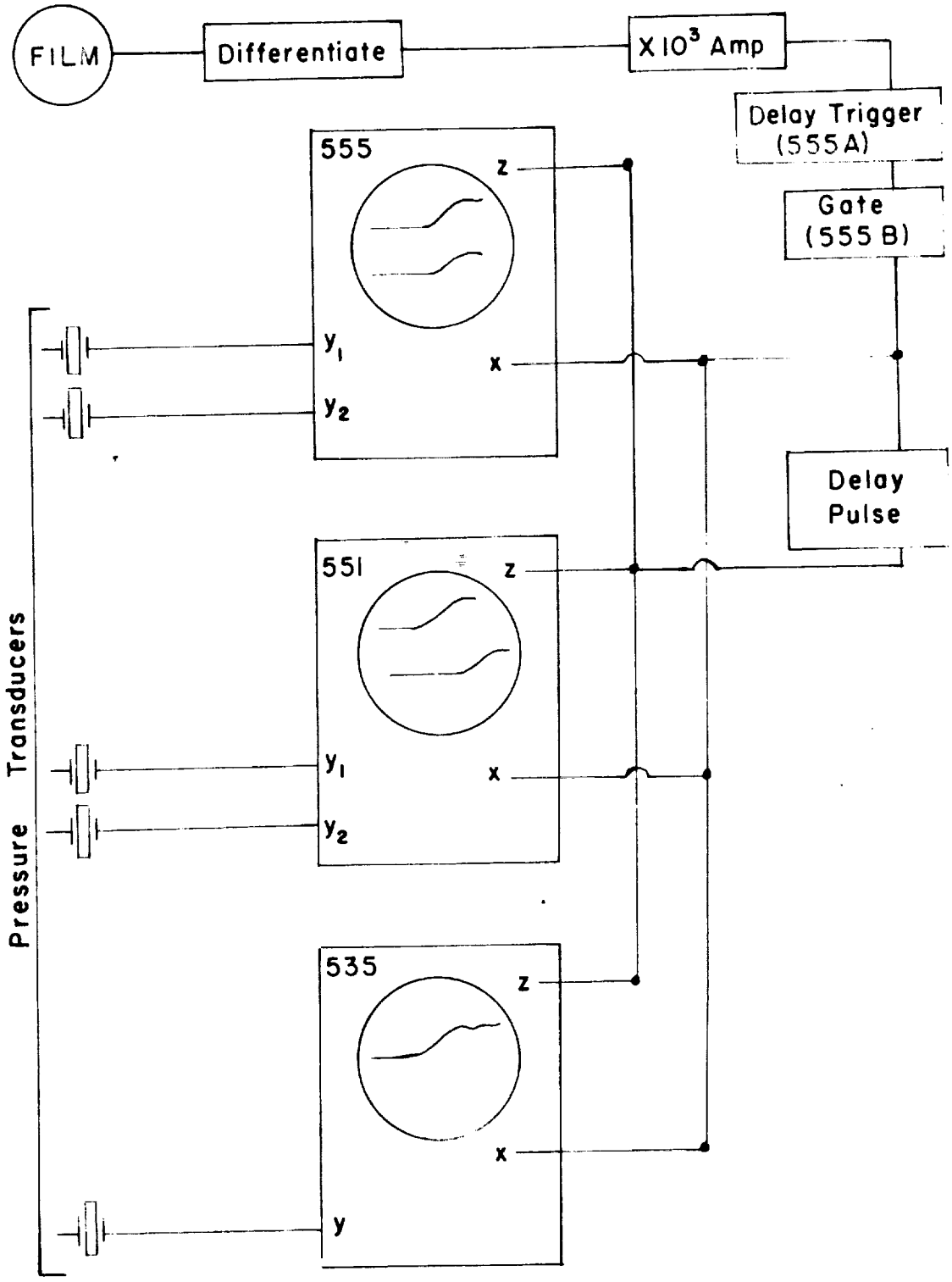

FIG. 5 INSTRUMENTATION FOR SHOCK CURVATURE MEASUREMENTS

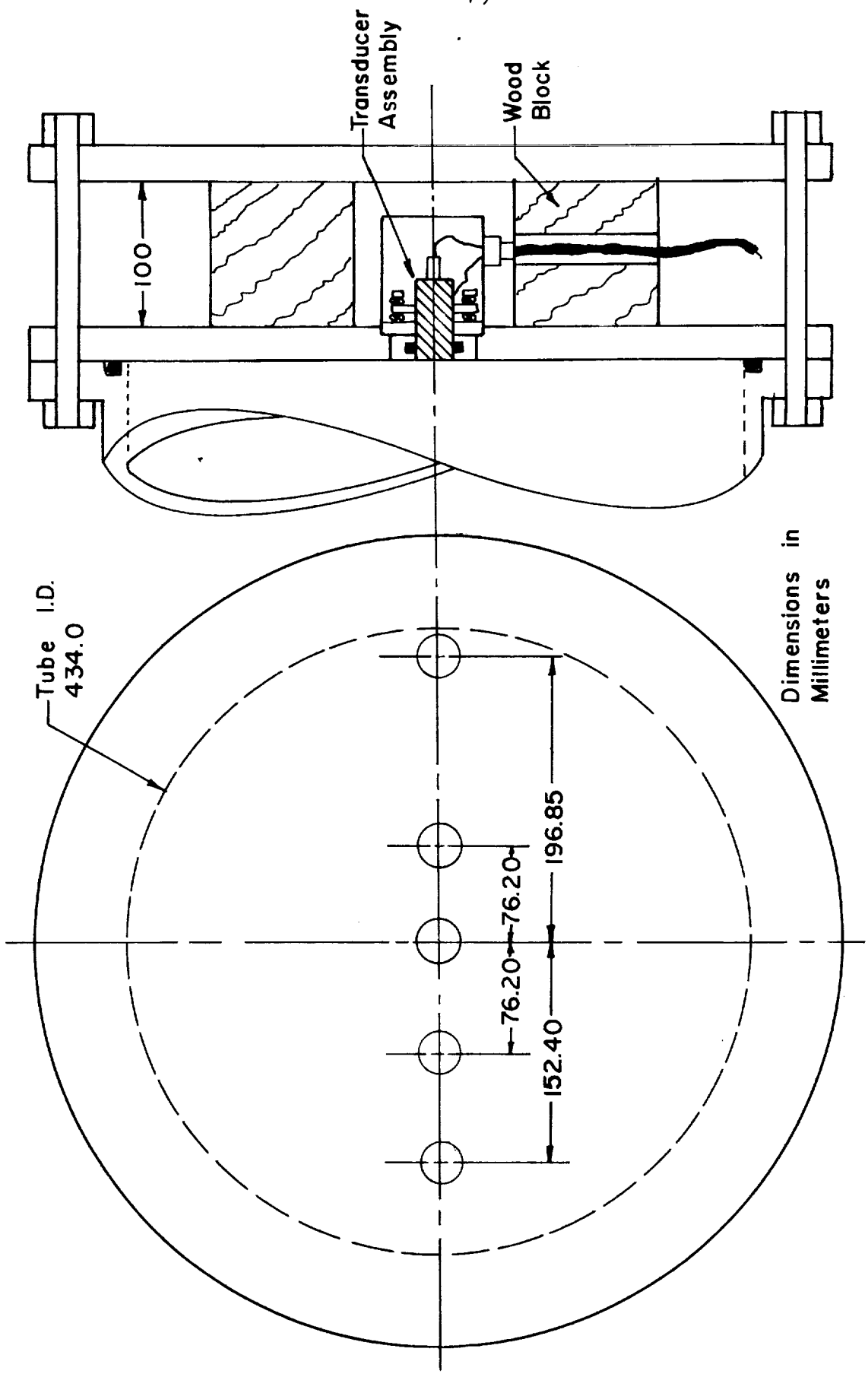

FIG. 6 END PLATE AND DAMPER INSTALLATION

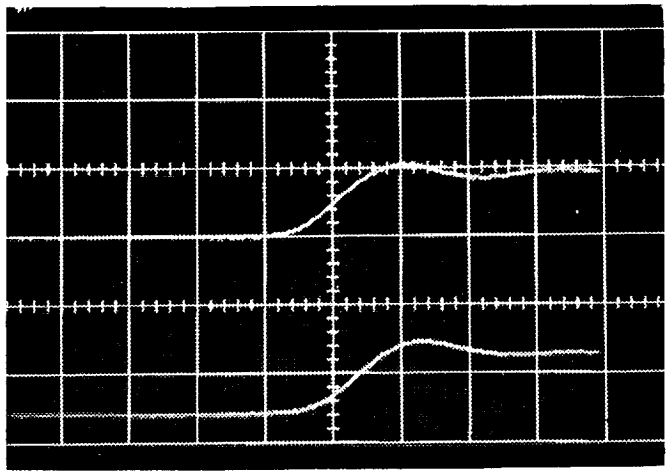

7a. Δp = 40 mm Hg
5 mv/cm; 1 μsec/cm
Air: p_1 = 60 μ Hg

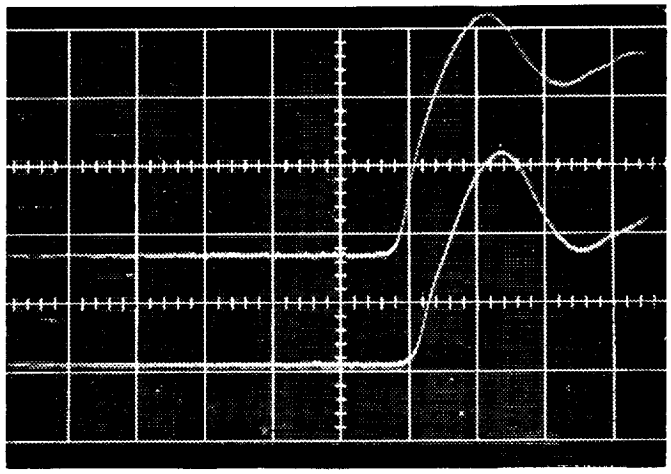

7b. Δp = 120 mm Hg
5 mv/cm; 1 μsec/cm
Air: p_1 = 240 μ Hg

FIG. 7. TYPICAL CALIBRATION TRACES

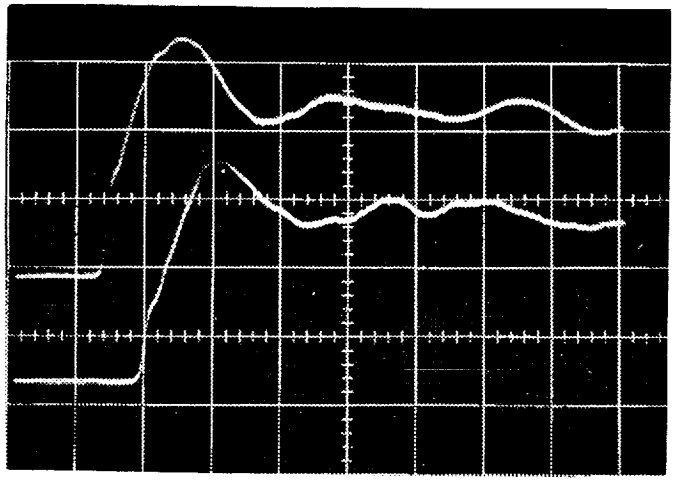

7c. Δp = 220 mm Hg
10 mv/cm; 1 μsec/cm
Air: p_1 = 575 μ Hg

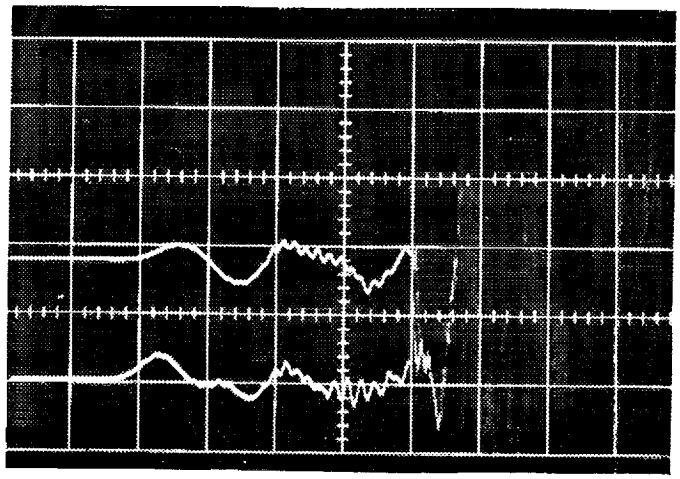

7d. "Galloping Zero"
p_4 = 24 psig; M = 7.73
10 mv/cm; 1000 μsec/cm

FIG. 7. TYPICAL CALIBRATION TRACES (continued)

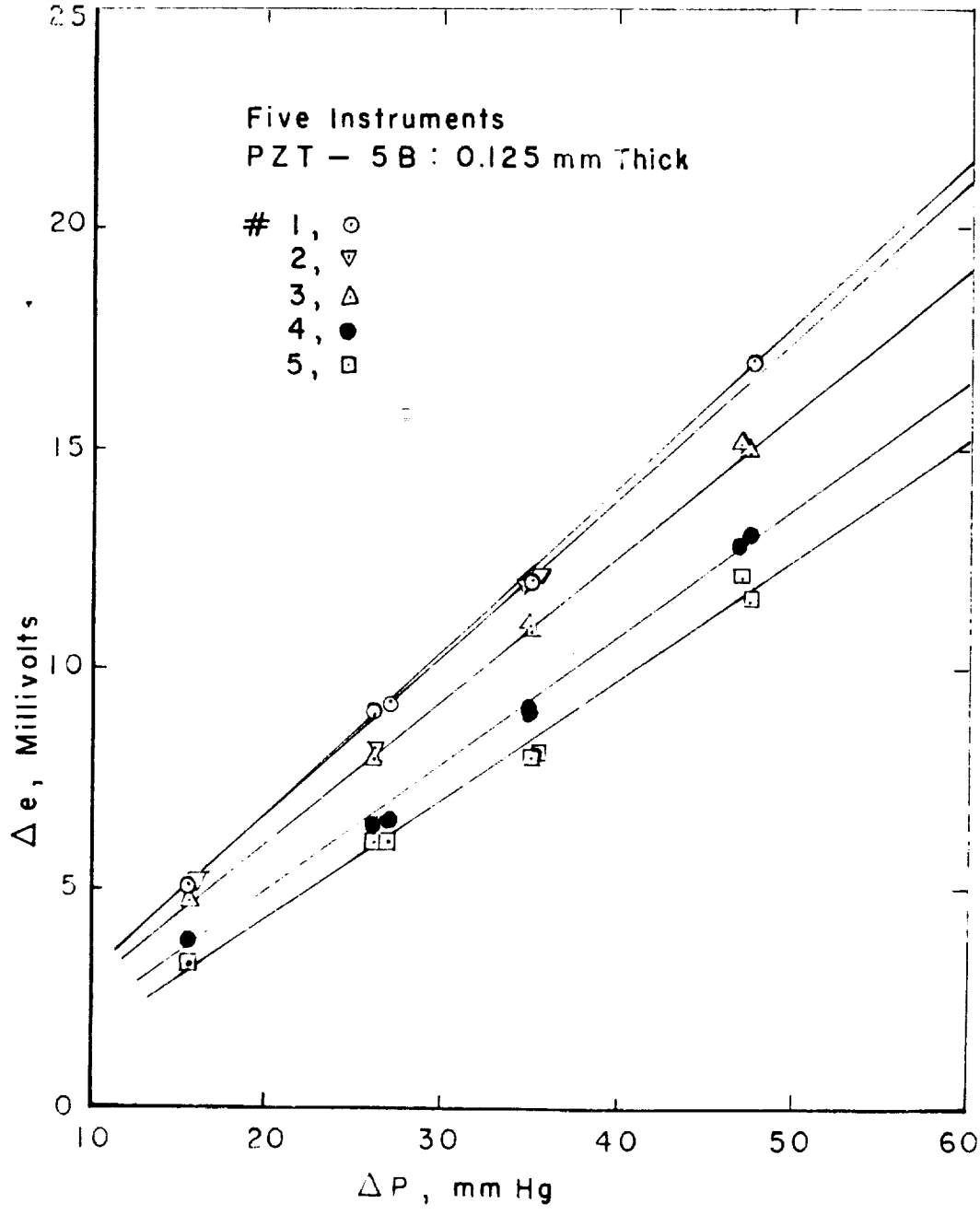

FIG. 8 TRANSDUCER CALIBRATIONS

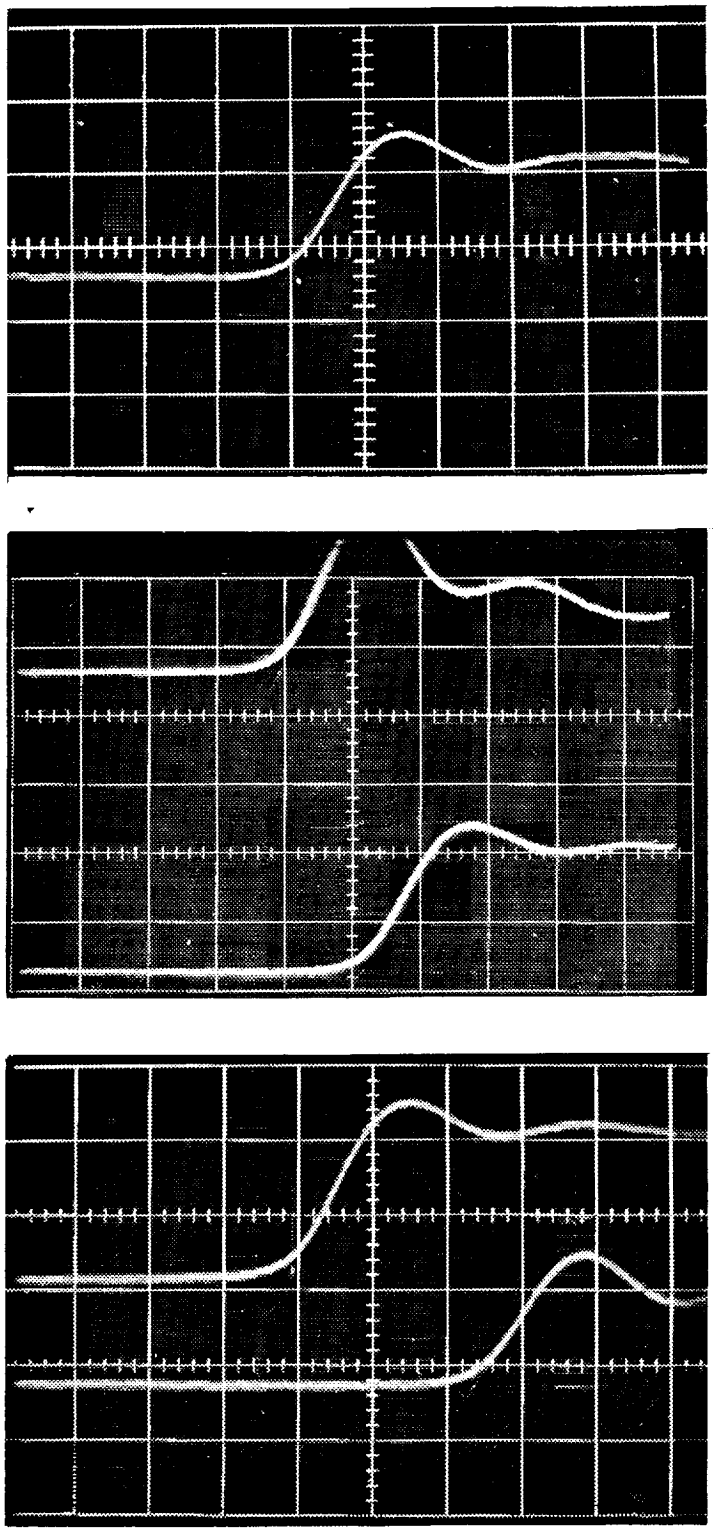

FIG. 9. TYPICAL CURVATURE TRACES

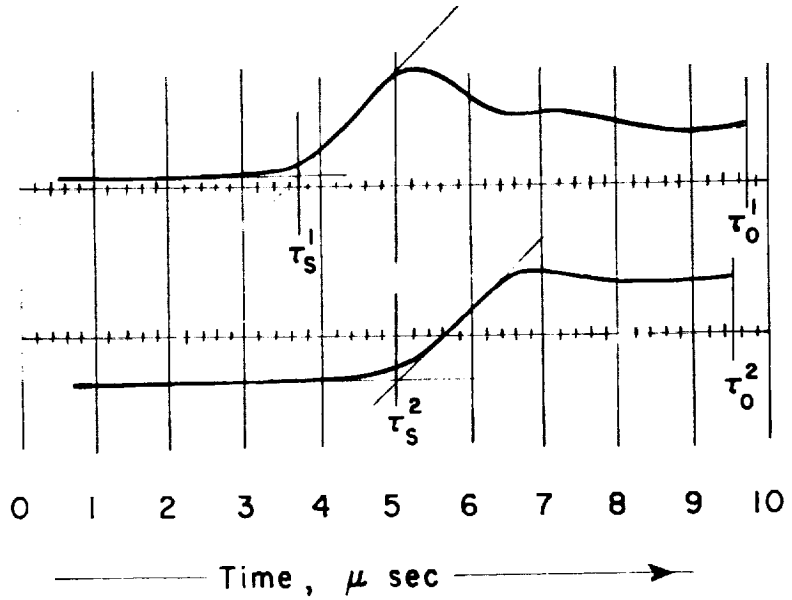

$$x_{12} = U_s \left[(\tau_s^2 - \tau_s^1) + (\tau_o^1 - \tau_o^2) \right]$$

(a) Shock Curvature

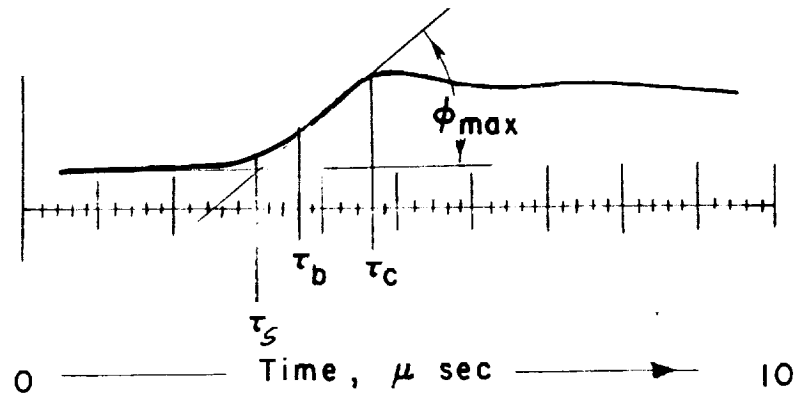

$$\delta_s = U_s \left[\tau_D + \tau_C - 2\tau_S \right]$$

(b) Shock Thickness

FIG. 10 MEASUREMENT TECHNIQUES

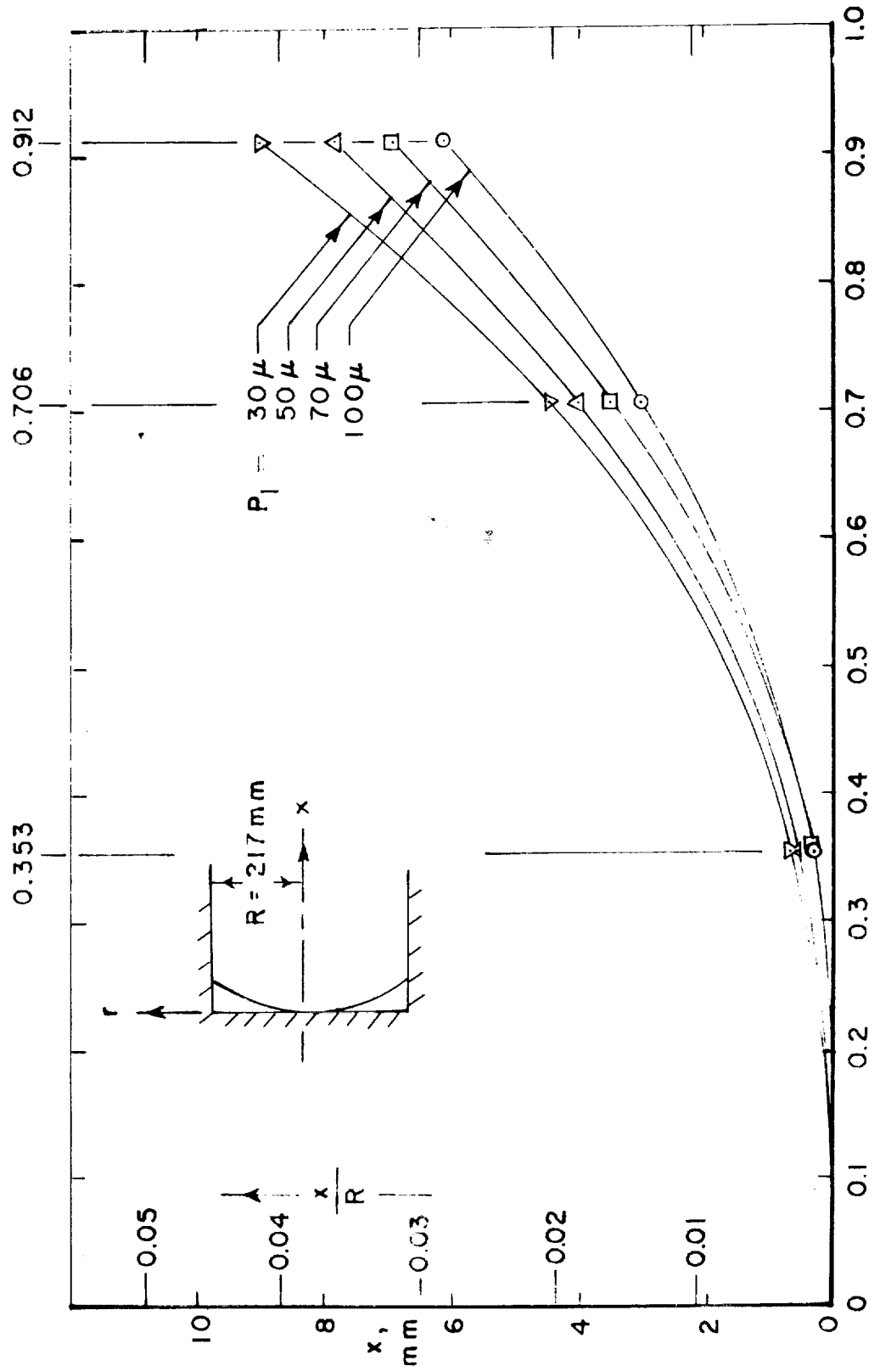

FIG. 11 TYPICAL SHOCK SHAPES

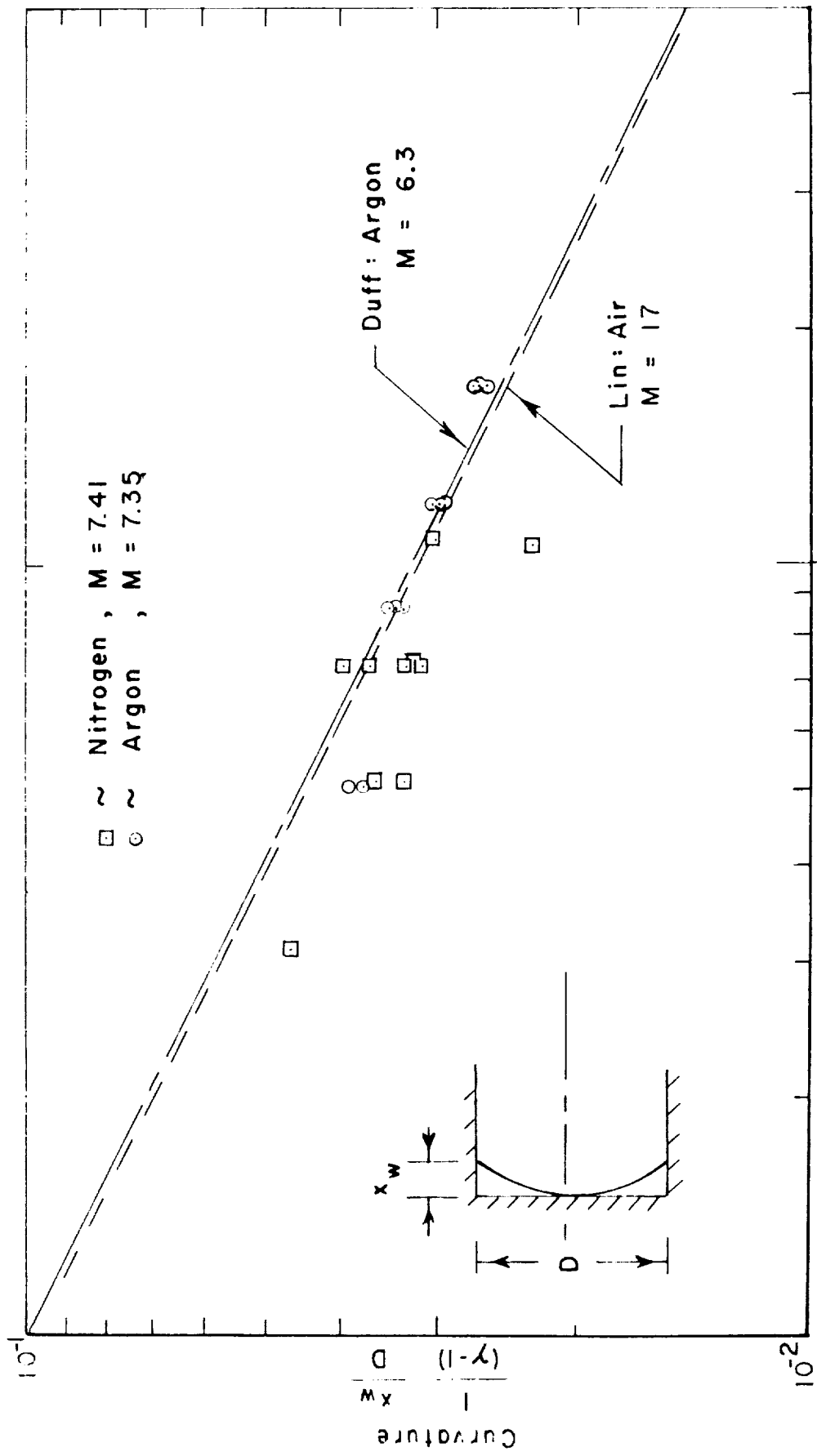

FIG. 12 TOTAL SHOCK CURVATURE

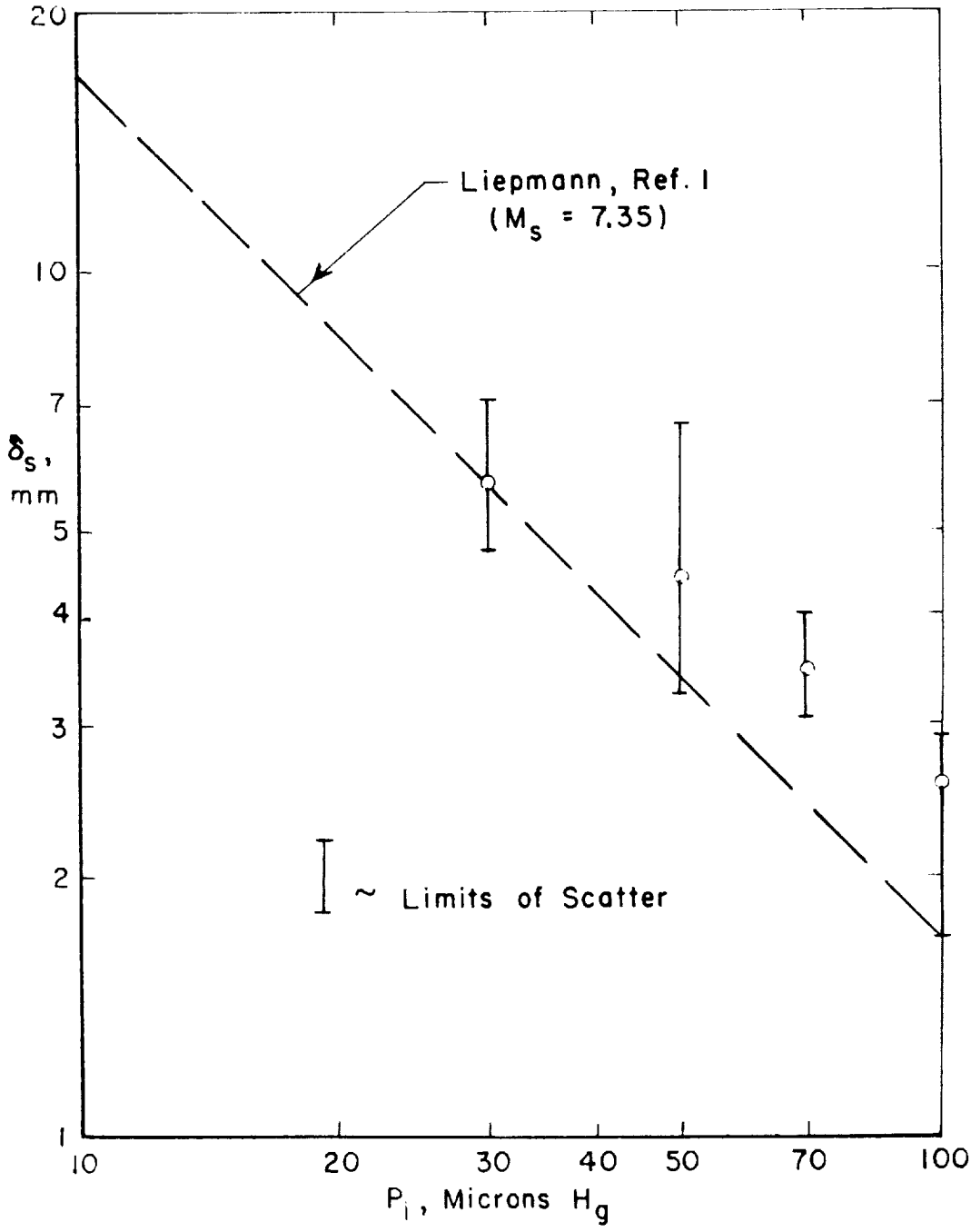

FIG. 13 SHOCK THICKNESS IN ARGON

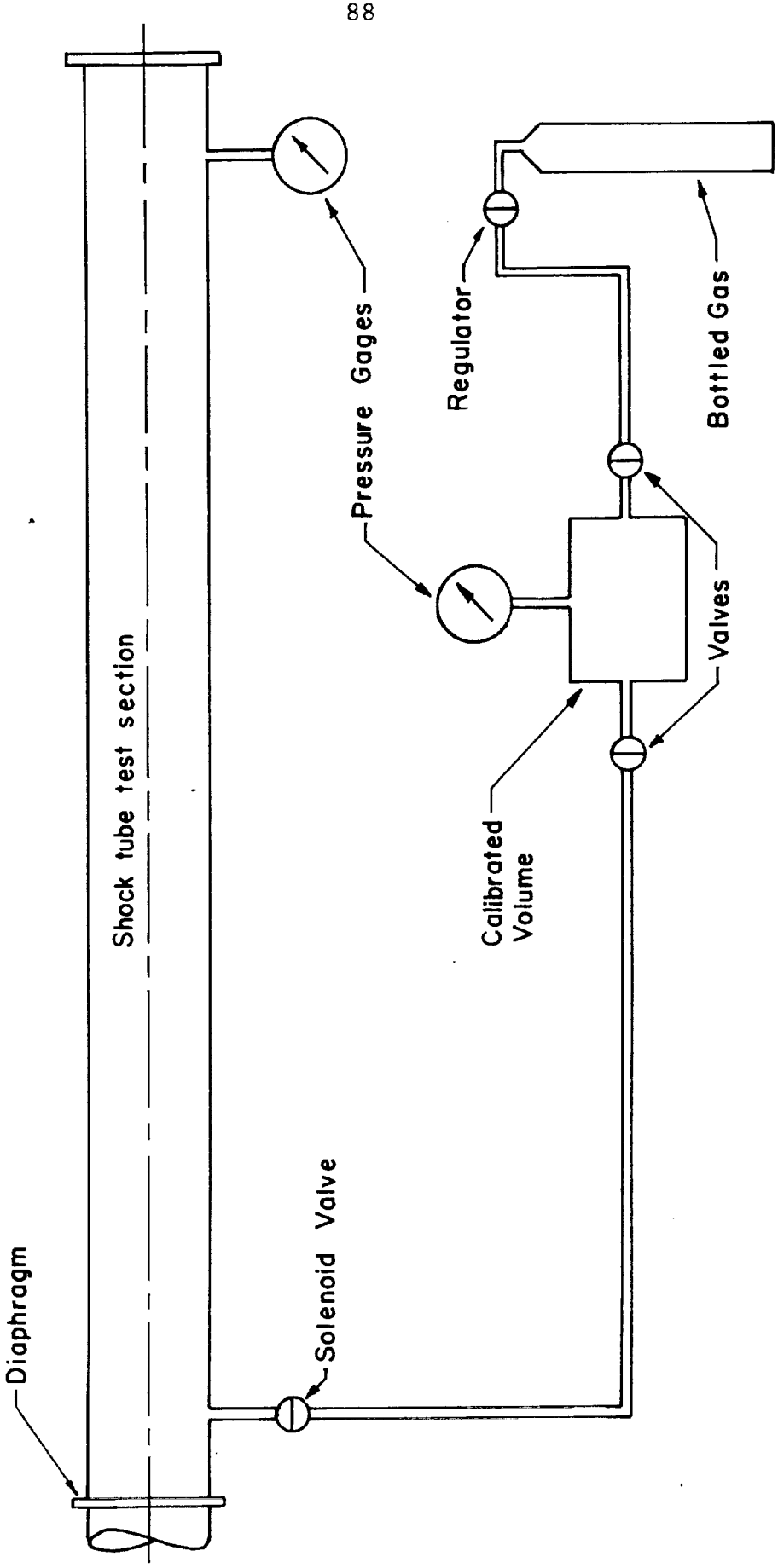

FIG.14 CALIBRATED TEST GAS INJECTION - SCHEMATIC

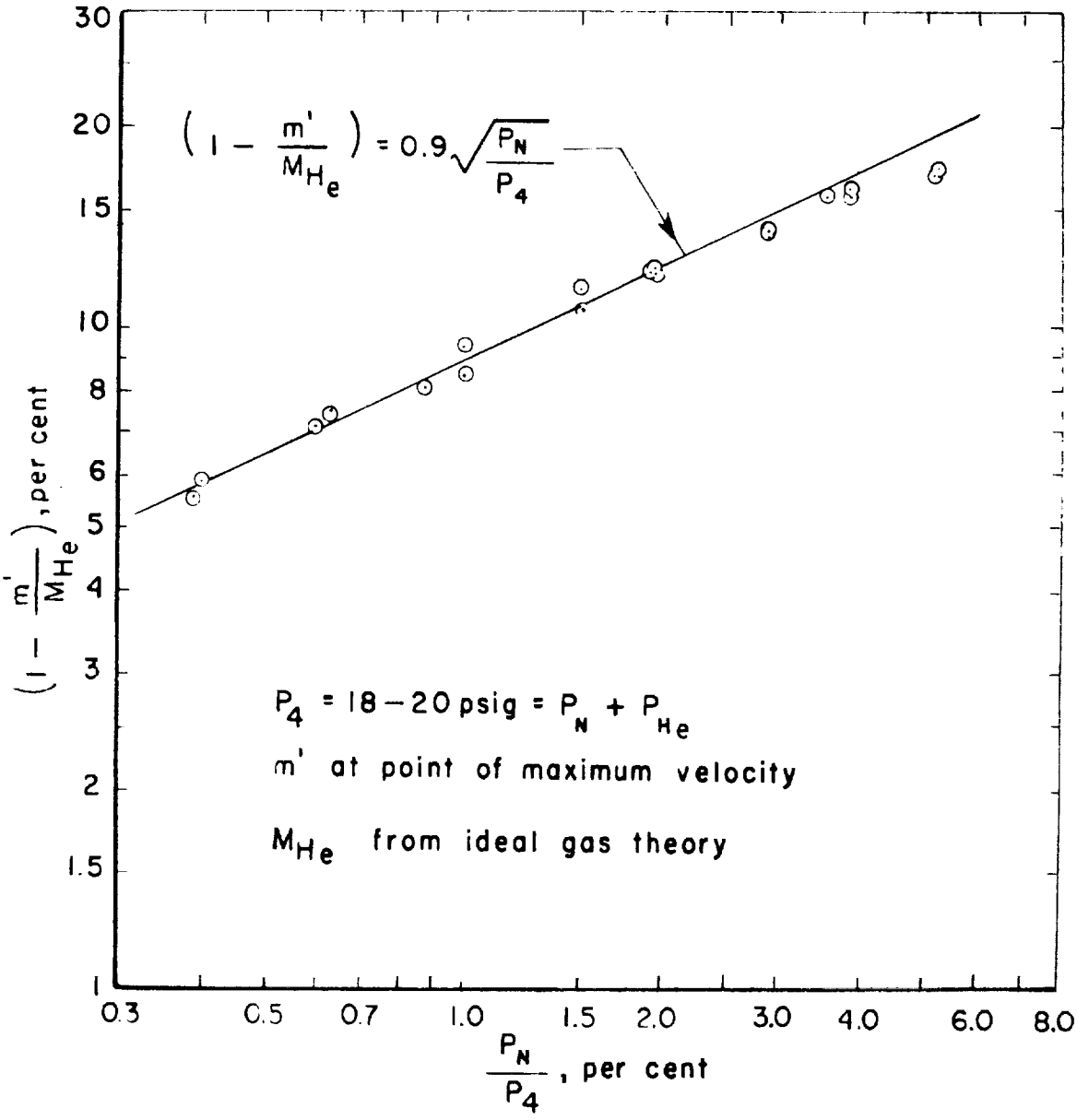

FIG. 15 DRIVER GAS MIXTURE TECHNIQUE